Development, Growth & Differentiation
The Japanese Society of Developmental Biologists

Develop. Growth Differ. (2012) **54**, 588–604 doi: 10.1111/j.1440-169X.2012.01362.x

Original Article

Establishment and characterization of Roberts syndrome and SC phocomelia model medaka (*Oryzias latipes*)

Akihiro Morita,[1,*,†] Kumiko Nakahira,[1] Taeko Hasegawa,[1] Kaoru Uchida,[1] Yoshihito Taniguchi,[2,‡] Shunichi Takeda,[2] Atsushi Toyoda,[3,§] Yoshiyuki Sakaki,[3,¶] Atsuko Shimada,[4] Hiroyuki Takeda[4] and Itaru Yanagihara[1,*]

[1]*Department of Developmental Medicine, Research Institute, Osaka Medical Center for Maternal and Child Health, Izumi, Osaka,* [2]*Department of Radiation Genetics, Faculty of Medicine, Kyoto University, CREST, Japan Science and Technology Laboratory, Kyoto,* [3]*Sequence Technology Team, RIKEN Genomic Sciences Center, Yokohama, Kanagawa, and* [4]*Department of Biological Sciences, Graduate School of Science, University of Tokyo, Tokyo, Japan*

Roberts syndrome and SC phocomelia (RBS/SC) are genetic autosomal recessive syndromes caused by *establishment of cohesion 1 homolog 2* (*ESCO2*) mutation. RBS/SC appear to have a variety of clinical features, even with the same mutation of the *ESCO2* gene. Here, we established and genetically characterized a medaka model of RBS/SC by reverse genetics. The RBS/SC model was screened from a mutant medaka library produced by the Targeting Induced Local Lesions in Genomes method. The medaka mutant carrying the homozygous mutation at R80S in the conserved region of ESCO2 exhibited clinical variety (i.e. developmental arrest with craniofacial and chromosomal abnormalities and embryonic lethality) as characterized in RBS/SC. Moreover, widespread apoptosis and downregulation of some gene expression, including *notch1a*, were detected in the R80S mutant. The R80S mutant is the animal model for RBS/SC and a valuable resource that provides the opportunity to extend knowledge of ESCO2. Downregulation of some gene expression in the R80S mutant is an important clue explaining non-correlation between genotype and phenotype in RBS/SC.

Key words: *ESCO2*, *Oryzias latipes*, premature chromosomal separation, Roberts syndrome and SC phocomelia.

Introduction

Roberts syndrome (RBS) (Online Mendelian Inheritance in Man [OMIM] 268300) is a genetic autosomal recessive syndrome. RBS is characterized by intrauterine fetal death, failure to thrive, mental and growth retardation, microcephaly, cleft lip and palate, and symmetrical limb defects (Vega *et al.* 2010). Chromosomal abnormality, for example, premature centromere separation (PCS), in the metaphase RBS cell is also observed. Recently, we identified *establishment of cohesion 1 homolog 2* (*ESCO2*) as the gene responsible for RBS (Vega *et al.* 2005). Similar pathological features, although milder than RBS, are observed in SC phocomelia (SC) (OMIM 269000). SC is also an autosomal recessive disorder caused by *ESCO2* mutation (Schüle *et al.* 2005). In spite of the mutation being in the same gene, different diagnoses were previously made. Both RBS and SC were caused by truncating mutations (either nonsense mutation or frame-shift), eliminating the functionally important acetyltransferase domain, except for one family in which RBS was caused by the missense mutation in the acetyltransferase domain (Schüle *et al.* 2005; Vega *et al.* 2005, 2010; Gordillo *et al.* 2008). Gordillo *et al.* (2008) considered that RBS and SC were the same syndrome with varying phenotypic expression. Thus, clinical

*Authors to whom all correspondence should be addressed.
Email: morita-a@suzuka-u.ac.jp; itaruy@mch.pref.osaka.jp
†Present address: Faculty of Pharmaceutical Sciences, Suzuka University of Medical Science, Suzuka, Mie 513-8670, Japan.
‡Present address: Department of Preventive Medicine and Public Health, School of Medicine, Keio University, Shinjuku-ku, Tokyo 160-8582, Japan.
§Present address: Comparative Genomics Laboratory, Center for Genetic Resource Information, National Institute of Genetics, Mishima, Shizuoka 411-8540, Japan.
¶Present address: Toyohashi University of Technology, Toyohashi, Aichi 441-8580, Japan.
Received 28 September 2011; revised 25 April 2012; accepted 9 May 2012.

features are considerably different in severity, suggesting there is no phenotype–genotype correlation.

The expression of *ESCO2* is dependent on the cell cycle, namely, it is expressed in the S-phase (Whitfield *et al.* 2000; Nishihara *et al.* 2010). *ESCO2* is a homologue of *Ctf7/Eco1* in the yeast *Saccharomyces cerevisiae* (Hou & Zou 2005). *ESCO2* and *Eco1* encode a member of the acetyltransferase family (Skibbens *et al.* 1999; Vega *et al.* 2010). The ECO1 protein lacks the N-terminal half of ESCO2. ECO1 and the C-terminal half of ESCO2 contain a PIP box, a C2H2 zinc finger and an acetyltransferase domain. PIP box and C2H2 zinc finger domains are involved in the interaction with proliferating cell nuclear antigen (Moldovan *et al.* 2006) and acetylation of cohesin subunits (Ivanov *et al.* 2001; Hou & Zou 2005; Rolef Ben-Shahar *et al.* 2008; Unal *et al.* 2008; Zhang *et al.* 2008; Onn *et al.* 2009), respectively. Cohesin acetylation by ESCO2 and ECO1 is a central determinant of replication fork processivity (Terret *et al.* 2009) and is essential for the establishment of cohesion from yeast to humans (Skibbens *et al.* 1999; Hou & Zou 2005).

Medaka (*Oryzias latipes*) and zebrafish (*Danio rerio*) are attractive vertebrate animal models because of their easy handling and large numbers of progeny per generation. To analyze gene function, an easy knockdown method using a morpholino injection has been established. Furthermore, medaka is suitable for genetic analysis because it has a lower ploidy level than zebrafish (Ishikawa 2000), and a high quality draft genome sequence of medaka (Kasahara *et al.* 2007) and large numbers of mutants (Furutani-Seiki *et al.* 2004) are available. In this study, we employed a reverse genetic approach in mutant medaka (*O. latipes*) produced using the Targeting Induced Local Lesions in Genomes (TILLING) method (Taniguchi *et al.* 2006) for translational research to explain RBS/SC pathobiology through the *ESCO2* mutation. The expression pattern of *ESCO2* in medaka is similar to that in humans. *ESCO2* mutant medaka showed RBS/SC-like divergence in their phenotype. This *ESCO2* mutant medaka is the animal model for RBS/SC. Moreover, downregulation of *notch1a* and its downstream gene expression was observed in *ESCO2* mutants. This is an important clue explaining the clinical variety of RBS/SC.

Materials and methods

Fish strain and embryos

This study was performed using K-Cab, a substrain of Cab, and K-Kaga, a northern strain of medaka. K-Kaga was a kind gift from the National BioResource Project Medaka. The mutant strains were derived from K-Cab (Taniguchi *et al.* 2006). Eggs were collected from a laboratory colony. Embryos were incubated at 28.5°C after collection, and were staged according to Iwamatsu (1994).

Cloning of medaka ESCO2

A partial cDNA sequence of medaka *ESCO2* was obtained from a genome database (University of Tokyo Genome Browser Medaka [http://utgenome.org/medaka/]), and was amplified using the primers (*ESCO2* cloning primers, see Table S1). Because the 5′ part was missing from the database, rapid amplification of 5′ cDNA ends (5′-RACE) was performed using the SMART RACE cDNA Amplification Kit (Clontech). Two rounds of 5′-RACE were performed with cDNA prepared from embryos using the gene-specific primers (*ESCO2* RACE primers, see Table S1). The cDNA fragment of *ESCO2* (5′-untranslated region and open reading frame [ORF]) was amplified by polymerase chain reaction (PCR) from embryonic cDNA library using *ESCO2* full forward and reverse as primers, and was cloned into pSTBlue-1 vector (Novagen).

In situ *hybridization*

cDNA sequences of medaka *β-actin*, *Ifng* and *myf5* were obtained from a genome database (Ensembl genome browser in medaka [http://uswest.ensembl.org/Oryzias_latipes/Info/Index]; accession no., *β-actin*, ENSORLT00000017152; *Ifng*, ENSORLT00000005779; *myf5*, ENSORLT00000020353). cDNA fragments were cloned into pSTBlue-1 (Novagen) vector by reverse transcription (RT)–PCR using each primer set (see Table S1) and sequenced for confirmation. The other genes were previously cloned into vectors (Kage *et al.* 2004). The RNA probes were produced by *in vitro* transcription by using SP6, T7 or T3 RNA polymerase (Roche Applied Science) and DIG RNA Labeling Mix (Roche Applied Science) according to the manufacturer's instruction. Whole-mount *in situ* hybridization was performed as previously described (Terasaki *et al.* 2006). The fixative solution was modified as follows: 4% paraformaldehyde (PFA) in 0.85× phosphate-buffered saline containing Tween-20 (0.1%, 0.85× PBST) and 1.5× PBST, which were used for the embryos at the gastrula stage (stage 16) and at other stages, respectively. The length of proteinase K treatment was modified as follows: 0, 1, 7 and 12 min for the embryos at stage 11 or earlier, 12–18, 19–24 and 25 or later, respectively. The samples were observed using a microscope (Olympus BX51).

Cartilage staining

Cartilage staining was performed according to Yasutake *et al.* (2004). The whole-mount and pectoral fin samples were observed by using a stereoscopic microscope (Olympus SZX10) and a microscope (Olympus BX51), respectively.

Immunohistochemistry

Immunohistochemical analysis was performed according to Iijima and Yokoyama (2007) by using anti-phosphorylated histone H3 antibody (Upstate, at 1/100 dilution) and Alexa Fluor 488 anti-rabbit immunoglobulin (Ig)G antibody (Invitrogen, at 1/1000 dilution). The samples were observed by using a fluorescence microscope (Olympus IX71).

5-Bromodeoxyuridine (BrdU) incorporation

Because medaka chorion is almost impermeable to BrdU (Nguyen *et al.* 1999), we injected 0.1% BrdU (in the kit FITC BrdU Flow Kit, BD Biosciences)/Yamamoto solution into the perivitelline space at 2.0 days postfertilization (dpf). Two hours after injection, the embryos were fixed by 4% PFA/PBST. After fixation, the experimental procedure was the same as in immunohistochemistry, but using anti-BrdU antibody (Thermo Scientific, at 1/500 dilution) and Alexa Fluor 488 anti-mouse IgG antibody (Invitrogen, at 1/1000 dilution).

Terminal deoxynucleotidyl transferase-mediated dUTP nick end labeling (TUNEL) assay

A whole-mount TUNEL assay was performed by using an *in situ* Apoptosis Detection Kit (Takara) according to the method of Iijima and Yokoyama (2007) and the manufacturer's instructions. The method was slightly modified as follows: The anti-fluorescein isothiocyanate (anti-FITC) antibody conjugated with horseradish peroxidase in the kit was replaced by anti-FITC antibody conjugated with alkaline phosphatase (at 1/500 dilution), 4-nitro blue tetrazolium chloride (NBT) and 5-bromo-4-chloro-3-indolyl-phosphate, 4-toluidine salt (BCIP) (Roche Applied Science) were used for visualization of apoptotic cells. The samples were observed by using a microscope (Olympus BX51).

Genotyping

Genomic DNA was extracted from whole embryos and caudal fin of fry by treatment of proteinase K (100 μg/mL proteinase K, 10 mmol/L Tris-HCl (pH 8.0), 5 mmol/L ethylenediaminetetraacetic acid, 1% sodium dodecylsulfate), phenol extraction, phenol-chloroform isoamyl alcohol extraction and isopropyl alcohol precipitation. The genomic DNA was subjected to PCR by using a primer set (*ESCO2* Seq1 and *ESCO2* Seq2, see Table S1). After confirmation of amplicon length by separation electrophoresis in agarose gel, PCR products was subjected to direct sequence by using BigDye Terminator (Applied Biosystems), and primers *ESCO2* Seq3 or *ESCO2* Seq2 (see Table S1).

Investigation of the expression allele of ESCO2

First we crossed *ESCO2*$^{240T,\ 242A,\ 581C/240G,\ 242T,\ 581C}$ females and *ESCO2*$^{240G,\ 242A,\ 581A/240G,\ 242A,\ 581A}$ males. At several developmental stages, total RNA extraction by ISOGEN (Nippon Gene) and DNase (in the kit of SV Total RNA Isolation System, Promega) treatment and first strand cDNA production (PrimeScript 1st strand cDNA Synthesis Kit, Takara) was carried out according to the manufacturer's instructions. The first strand cDNA was subjected to PCR using TaKaRa Ex Taq (Takara) and the primer set (*ESCO2* full, see Table S1). The PCR products were separated by agarose electrophoresis. Direct sequencing was performed using the primer *ESCO2* Seq4 or *ESCO2* Seq3 (see Table S1). From the sequence, we assessed the expression alleles as follows: when the nucleotide sequence is 240T/G, 242A/T and 581C, the RNA is derived from two maternal alleles; when it is 240T/G, 242A/T and 581C/A, the RNA is from two maternal and paternal alleles; and when it is 240T/G, 242A and 581C/A or 240G, 242T/A and 581A/C, the RNA is from one maternal and paternal (i.e. embryonic alleles).

Morpholino injection

We constructed three morpholinos as follows: ATG mo, CGGATCATCTTCAGAGTTCACCGTC (start codon underlined); 5mis mo, CGCATGATCTTCACAGTTGACCCTC (mispaired bases underlined); and E2I2 mo, GCTTCCAGGAACCTCCGTACCTGTC (targets 3′-donor of exon 2). Morpholinos (50–300 nmol/L) diluted with Yamamoto solution were injected into one blastomere of one-cell stage embryos (stage 2) using FemtoJet (Eppendorff) and Injectman M2 (Eppendorff) according to the method of Rembold *et al.* (2006) under a stereoscopic microscope (Olympus SZX7).

Chromosomal analysis

Chromosomal analysis was performed according to the method of Westerfield (2000). Briefly, colchicine-treated (400 μg/mL at 28.5°C for 180 min) embryos

were treated with 1.1% trisodium citrate for 16 min. During trisodium citrate treatment, embryos were dechorionated and the yolk was dissected away. After hypotonization (50 mmol/L KCl at 30°C for 15 min), the dissociated cells were fixed using cold Carnoy's fixative for 20 min and washed. The fixed cell solution was divided into two aliquots. One of them was subjected to DNA extraction and genotyping (see genotyping). The other was spotted onto a cold slide glass and re-fixed by flame. The samples were stained using Giemsa solution (4% Giemsa Stock in 10 mmol/L phosphate buffer for 60 min, pH 7) and observed using a microscope (Olympus BX51).

Flow cytometry

Sample preparation was as previously described (Candal *et al.* 2007), but slightly modified. Briefly, after filtration of nuclei from frozen and dechorionized embryos, filtrates were treated with RNase A (100 μg/mL; Wako) and stained with 1 mg/mL propidium iodide (Dojindo). Nuclei (10 000) were analyzed using FACScan (BD Biosciences).

Quantitative RT-PCR

cDNA sequences of *notch1a*, *notch1b*, *notch3*, *ascl1a*, *ascl1b*, *GATA-1* and *EF-1α* were obtained from a genome database (Ensembl genome browser in medaka [http://uswest.ensembl.org/Oryzias_latipes/Info/Index]; accession no.: *notch1a*, ENSORLT00000006535; *notch1b*, ENSORLT00000000793; *notch3*, ENSORLT00000007526; *ascl1a*, ENSORLT00000020662; *ascl1b*, ENSORLT00000015163; *GATA-1*, ENSORLT00000017528; and *EF-1α*, ENSORLT00000009544). cDNA sequences of *sox9b*, *col2a1a* and *col2a1b* were obtained from GenBank (accession no.: *sox9b*, AY870393; *col2a1a*, AB617801; *col2a1b*, AB617803). Total RNA extraction and first strand cDNA production were carried out as described above. Before RT–PCR analysis, we performed sequence analysis of *ESCO2* similar to that performed during the investigation of expression alleles. For quantification of mRNA of *notch1a*, *notch1b*, *notch3*, *ascl1a*, *ascl1b*, *GATA-1* and *EF-1α*, real-time PCR analysis was applied to the first strand cDNA and the plasmid vector containing the target gene (as standard) using Applied Biosystems 7500 Fast RT–PCR System (Applied Biosystems), QuantiTect SYBR Green PCR Kit (Qiagen) and primer sets (see Table S1). For quantification of mRNA of the *sox9b*, *col2a1a* and *col2a1b*, Custum TaqMan Gene Expression Assays (assay name and ID: MFSOX9B, AIGJP3B; MFCOL2A1A, AIHSN9J; MFCOL2A1B, AII1MFR; Applied Biosystems) was used. After estimating the amount of mRNA from the cycle threshold (Ct) value of samples and the standard curve, the amount of mRNA was normalized by the amount of *EF-1α* mRNA and represented by relative abundance against wild-type (WT) embryos. Some amplified fragments were cloned into pT7Blue vector (Novagen) and were sequenced for confirmation.

Statistical analysis

Several statistical analyses were performed according to Zar (2010).

Results

Cloning of medaka ESCO2 *cDNA*

We cloned medaka *ESCO2* cDNA (DNA Data Bank of Japan accession no. AB601774) from embryos. It had a 1590-bp ORF encoding a 530-residue polypeptide, and a 5′-non-coding region of 177 nucleotides. The predicted ESCO2 had a calculated molecular weight of 58.7 kDa. The similarity searches showed that the medaka ESCO2 protein was similar to ESCO2 from several species including humans (Fig. S1). The identities of the medaka ESCO2 protein to that of humans, mice and zebrafish were 52.6%, 55.8% and 47.8%, respectively. Medaka ESCO2 had several conserved regions that consisted of a nuclear localization signal, PIP domain, C2H2-zinc finger domain, acetyltransferase domain and regions with unknown functions.

Expression pattern of ESCO2 *in medaka*

We investigated the *ESCO2* expression pattern during embryogenesis using whole-mount *in situ* hybridization. *ESCO2* mRNA was detected in all blastomeres at stage 5 (Fig. S2) and in the embryonic shield during gastrulation (stage 15–16, Fig. 1A). During early somitogenesis stages, *ESCO2* was expressed throughout the embryonic body, particularly in the optic vesicles, neural tube and somites (Fig. 1B). *ESCO2* expression was limited to the posterior region of optic tectum, prospective corpus cerebelli and pectoral fin buds in late somitogenesis stages at and after stage 28 (Fig. 1C), and to the genital ridge at stage 31 (Fig. 1D). These results are similar to the *ESCO2* expression pattern in human embryos (Vega *et al.* 2010). Because these *ESCO2*-expressing regions are thought to be proliferative zones (Nguyen *et al.* 1999; Candal *et al.* 2007), we

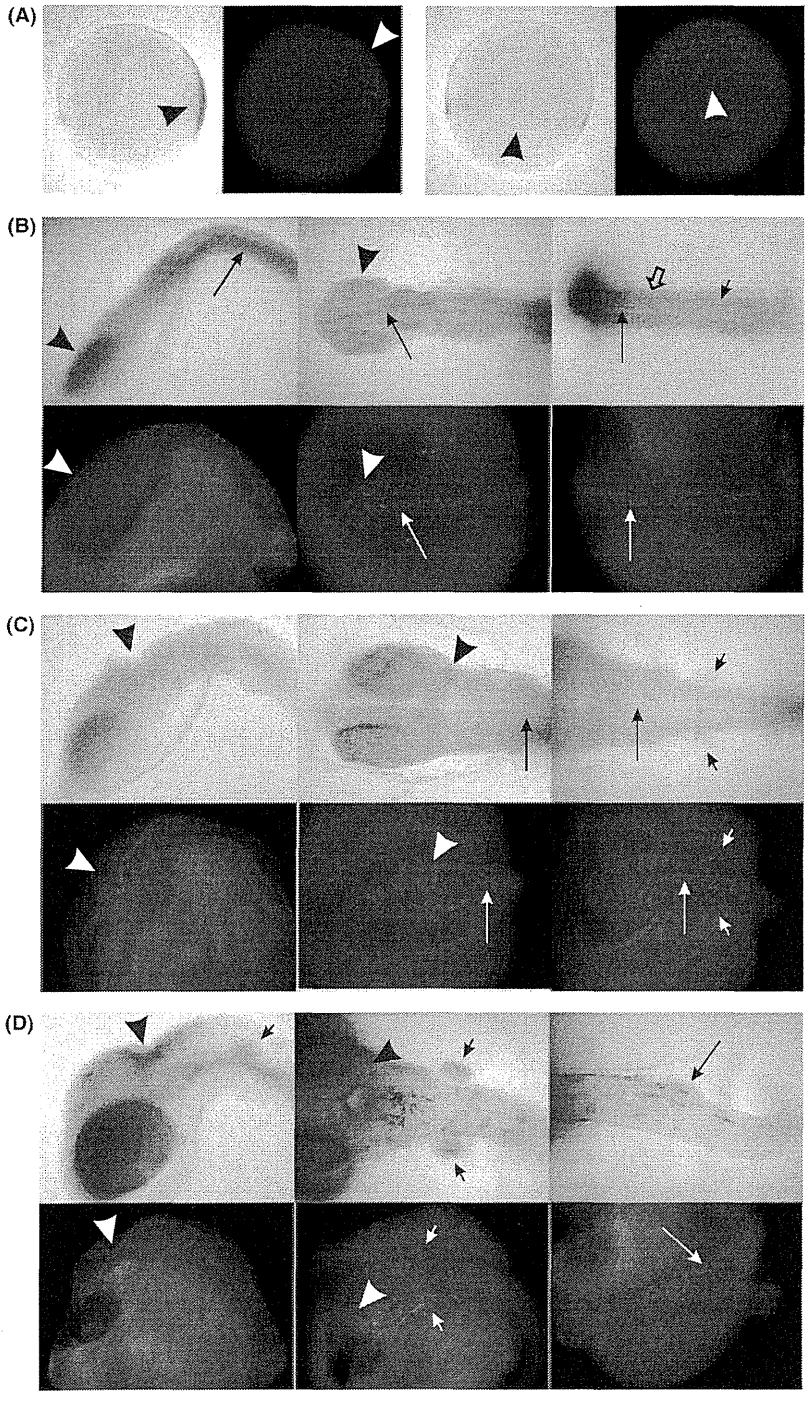

Fig. 1. *ESCO2* expression in medaka embryo. Whole-mount *in situ* hybridization analysis of *ESCO2* (micrograph) and immunohistochemical analysis of anti-phosphorylated histone H3 (M phase marker, fluorescence micrograph). (A) Gastrula stage (0.75 days postfertilization [dpf], stage 15). Left, lateral view; right, dorsal view; animal pole to top; arrowheads, embryonic shield. (B) Somitogenesis stage (1.0 dpf, stage 20). Left, lateral view; middle and right, dorsal view of head and tail, respectively; arrowheads, optic vesicles; long arrows, neural tube; open arrow, somite; short arrow, bilateral region in presomitogenic region. (C) Late somitogenesis stage (2.0 dpf, stage 28). Left, lateral view; middle and right, dorsal view of the head and pectoral regions, respectively; arrowheads, proliferative zone of optic tectum and prospective corpus cerebelli; long arrows, neural tube; short arrows, pectoral fin buds. (D) Gill blood vessel formation stage (3.0 dpf, stage 31). Left, lateral view; middle, dorsal view of the pectoral region; right, right dorsal view of abdomen; arrowheads, proliferative zone of optic tectum and prospective corpus cerebelli; short arrows, pectoral fin buds; long arrows, genital ridge.

performed immunohistochemical analysis of phosphorylated-histone H3, an M-phase marker. The immunopositive region was similar to the *ESCO2*-expressing region. These observations are in agreement with the fact that *ESCO2* is involved in cell division in other species (Skibbens *et al.* 1999; Hou & Zou 2005; Vega *et al.* 2005).

Developmental abnormalities in ESCO2 *mutant medaka*

In order to establish the RBS/SC model using medaka, we isolated mutant medaka from the TILLING library (Taniguchi *et al.* 2006). On sequence analysis, 18 mutations, including six missense, seven silent and five

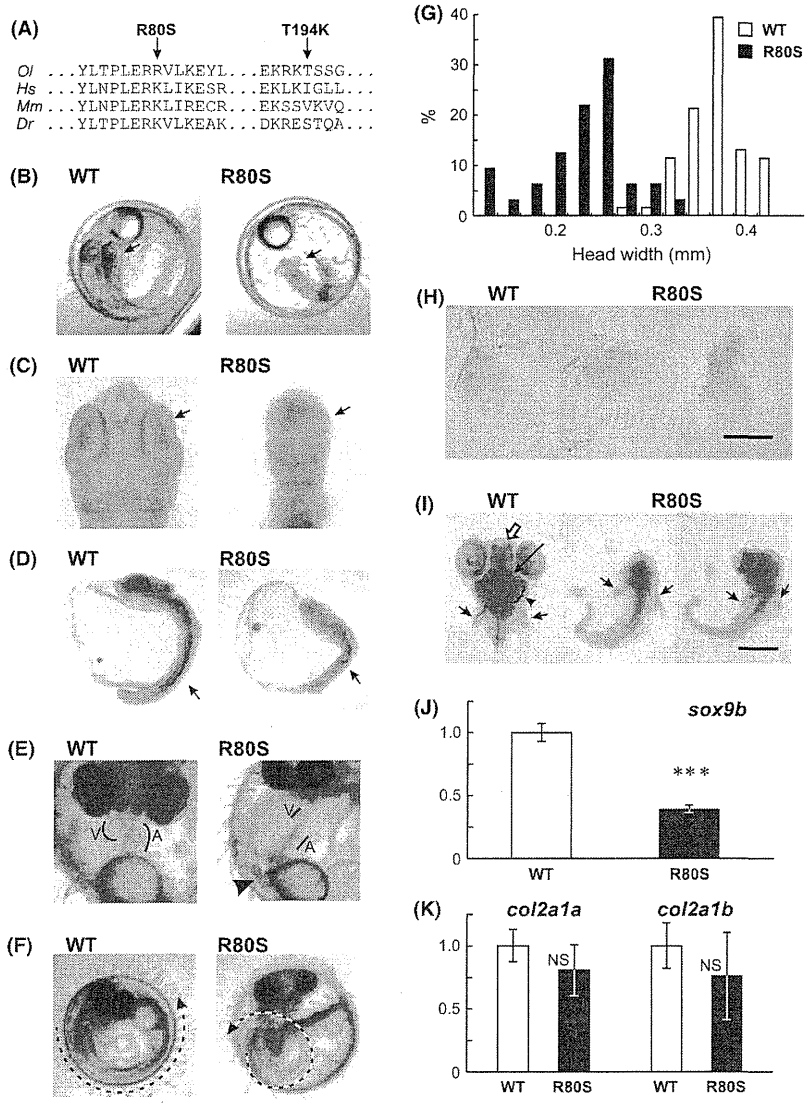

Fig. 2. Developmental abnormality of *ESCO2* mutant medaka. (A) Alignment of amino acid sequence of ESCO2 (R80 and T194 adjacent sequences). Note that R80 and adjacent region is conserved. *Ol*, *Oryzias latipes*; *Hs*, *Homo sapiens*; *Mm*, *Mus musculus*; *Dr*, *Danio rerio*. (B–C) Head deformity of R80S homozygous mutant (B, 2.5 days postfertilization [dpf] optical observation; C, 2.0 dpf whole-mount *in situ* hybridization [WISH] with *β-actin* probe). Note: small head and lack of eyes (arrows). (D) Somite malformation of R80S mutant (2.0 dpf WISH with *β-actin* probe). The number of somites was decreased and disarranged (arrows). (E) Heart malformation of R80S mutant (5.0 dpf). In mutant, defects in looping of heart and stagnation in the tail (an arrowhead) were observed. V, ventricle; A, atrium. (F) Body axis abnormality in R80S mutant (5.0 dpf). Dashed lines indicate body axis. (G) The head width of wild-type (WT) and R80S mutant (2.0 dpf). R80S mutants were significantly smaller than WT embryos ($P < 0.001$, $n = 32–61$). (H) Alcian blue staining of pectoral fin of WT and R80S mutant (6.0 dpf). Scale bar, 0.25 mm. In R80S mutants, the development of pectoral fins was normal (middle) or delayed (right). (I) Alcian blue staining of WT (head and pectoral region) and R80S mutant (whole body) (6.0 dpf, ventral view). In R80S mutant, defect of cartilage formation was observed. Open arrow, Meckel's cartilage; long arrow, ceratohyal; short arrow, pectoral fin; arrowheads, ceratobranchial arch. Scale bar, 0.5 mm. (J–K) *sox9b*, *col2a1a* and *col2a1b* expression in WT and R80S mutant (2.0 dpf) ($n = 13–14$). ***$P < 0.01$; NS, not significant; Student's *t*-test.

intronic *ESCO2* mutations were identified from 5760 clones. Among the six missense mutations, we selected R80S (240G→T, nucleotide) and T194K (581C→A, nucleotide) mutations for artificial insemination because R80 was highly conserved among species and T194K substitution confers the charged amino acid (Fig. 2A). Heterozygous (*ESCO2*$^{R80S/WT}$ and *ESCO2*$^{T194K/WT}$) embryos developed normally and did

Table 1. Genotyping and phenotype of *ESCO2* mutation[†]

Generation	*n*	*WT/WT* (%)	*R80S/WT* (%)	*R80S/R80S* (%)	Phenotype in R80S homozygous mutant (%)			
					Apparently normal	Developmental arrest[‡]	Cardiac abnormality	Body axis abnormality
F3[§]	73	30.1	53.4	16.4	100.0	0.0	0.0	0.0
F4[¶]	206	28.2	47.6	24.3	4.0	60.0	0.0	0.0
F5[††]	198	19.7	56.4	24.2	0.8	60.4	16.7	20.8

[†]Embryos and adults were progenies of heterozygous parents in all generations examined. [‡]Developmental arrest with craniofacial abnormalities and somite malformation by 2.0 days post fertilization (dpf). [§]Data of adults only. Embryonic development was not examined. [¶]F4 embryos (at stage 28, 2.0 dpf). [††]F5 embryos (by hatch). Sampling was carried out at appearance of abnormality. Cumulative value is shown.

not show pathological phenotypes. However, when the heterozygotes were intercrossed, the resulting *ESCO2*$^{R80S/R80S}$ homozygous mutants exhibited developmental delay and died before hatching. Homozygous *ESCO2*$^{T194K/T194K}$ embryos developed normally. Therefore, we further analyzed the R80S homozygous mutants in detail. Genotyping F3–F5 generation of backcrossed mutants (n = 73–206) showed that this mutation was transmitted in a Mendelian fashion (Table 1). The mutants developed normally during gastrulation and neurulation. From 1.5 dpf (stage 19), 60% of the mutants began to exhibit developmental delay. By 2.0 dpf (stage 28), their development was arrested (Table 1) and they were smaller than WT (Figs. 2G, S5A). The mutants showed head deformities (particularly brain and eye malformation, Fig. 2B,C) and somite malformation (Fig. 2D), both of which expressed *ESCO2* during the somitogenesis stages (Fig. 1). The rest of homozygous mutants developed normally until 2 dpf (hereafter called "escapers"). However they exhibited the heart abnormality (looping defect), stagnation (16.7% of mutants, Fig. 2E) and body axis malformation (20.8%, Fig. 2F) subsequently, and 91.7% of F5 mutants died by hatching period (Table 1), indicating that the homozygous mutation causes embryonic lethality. Because phocomelia and craniofacial abnormality are characterized in RBS/SC, we observed cartilage of mutants. The mutants were deficient in clear structure of cartilage. However, the pectoral fins were normally developed by 6.0 dpf in most mutants (Fig. 2H, middle). Some mutants showed developmental delay (Fig. 2H, right). The ventral cartilage elements of heads were almost defective in mutants by 6.0 dpf (Fig. 2I). Furthermore, the gene expression of *sox9b*, a transcriptional factor for cartilage formation, and *col2a1a* and *col2a1b*, components of cartilage, was examined at 2.0 dpf embryos. In mutants, *sox9b* was suppressed (Fig. 2J) but both *col2a1a* and *b* were not (Fig. 2K). At 2.0 dpf, the cartilage was not observed even in WT embryos (data not shown). Because the expression levels of *col2a1a* and *b* were very low, no significant difference between mutants and WT embryos may be observed.

It is known that ECO1 is essential for cellular viability in yeast (Skibbens *et al.* 1999). Although there are two related molecules in vertebrates, ESCO1 and ESCO2, each plays a distinct role and both are required for normal cell cycle progression (Hou & Zou 2005). To investigate the reason the homozygous mutants developed normally up to 1.5 dpf, we examined the effect of maternal mRNA accumulated in oocytes. To address this, we examined expression alleles using point mutation and polymorphism of *ESCO2* (Fig. S3). Until stage 14, *ESCO2* mRNA was derived from two maternal alleles. The paternal or embryonic *ESCO2* mRNA began to be expressed from stage 12, in agreement with the previous finding that midblastula transition of medaka begins at stage 11 (Aizawa *et al.* 2003). These data suggest that maternal mRNA of *ESCO2* caused normal development in R80S homozygous mutants during the early stages of development.

We attempted the rescue experiment by injection of WT *ESCO2* mRNA into mutant embryos. Unfortunately, we produced no detectable effects on phenotypes of mutants.

Almost all the mutations reported so far in RBS/SC patients are protein-truncating mutations (Schüle *et al.* 2005; Vega *et al.* 2005, 2010; Gordillo *et al.* 2008). Because the mutant we recovered from the TILLING library was the missense mutation, we constructed three morpholinos (Fig. S4), ATG mo (translation inhibitor), E2I2 mo (splicing inhibitor) and 5mis mo (control), and injected them into eggs immediately after fertilization to further investigate the role of ESCO2 in the embryogenesis. Because the maternal mRNA of *ESCO2* was accumulated until stage 14 as mentioned above, ATG mo was aimed at inhibiting both maternal and embryonic *ESCO2*, and E2I2 mo at inhibiting only embryonic *ESCO2*. The morpholinos had weak effect. Head deformities and somite malformation were not

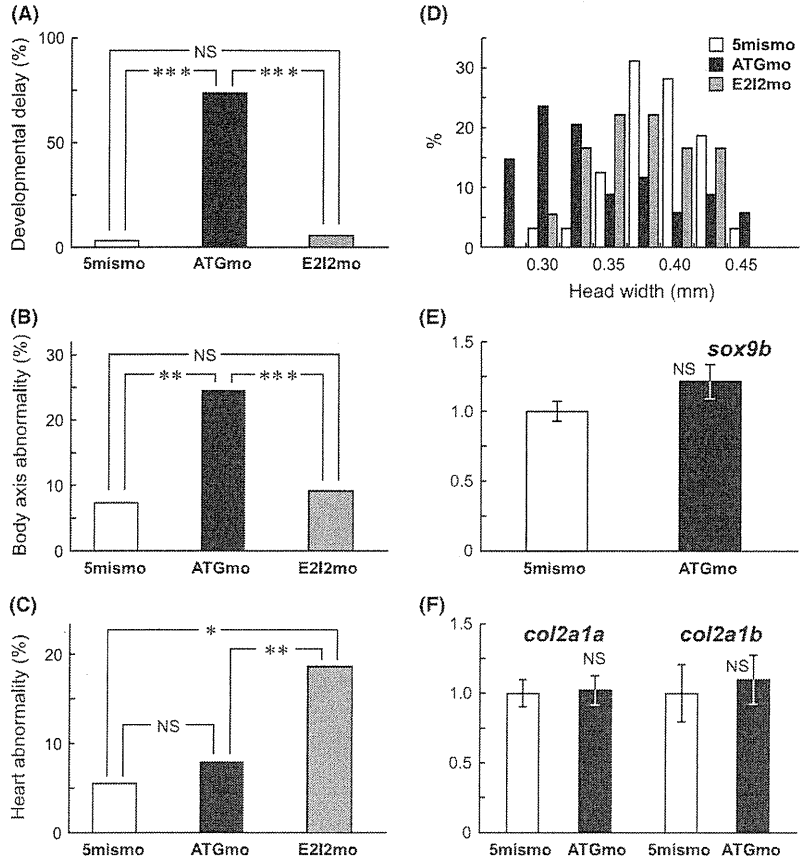

Fig. 3. Developmental abnormality of *ESCO2*-knockdown morphant. (A–D) The incidence of developmental delay (A), body axis abnormality (B, as in Fig. 2F) and heart malformation (C, as in Fig. 2E), and the head width (D) of morphants with 300 nmol/L of ATG mo (translation inhibitor, solid bars), E2I2 mo (splicing inhibitor, shaded bars) and 5mis mo (control, empty bars) injected just after fertilization. The 2.0-days postfertilization (dpf) embryos without heart beats were regarded as developmentally delayed. ATG mo morphants exhibited developmental delay. Body axis abnormality and heart malformation were observed by 5 dpf (n = 54–101). ATG mo morphants showed body axis abnormality. E2I2 mo induced heart malformation, but ATGmo did not. ***P < 0.001; **P < 0.01; *P < 0.05; NS, not significant; Tukey-type multiple comparison test (A–C); Tukey–Kramer test (D). ATG mo-injected morphants (2.0 dpf) were significantly smaller than control and E2I2 mo morphants (P < 0.001, n = 18–34). (E–F) *sox9b*, *col2a1a* and *col2a1b* expression in control and ATG mo morphants (2.0 dpf). NS, not significant; Student's t-test (n = 13).

obvious in morphants (data not shown). The expression of *sox9b*, *col2a1a* and *col2a1b* was not also affected in ATG mo morphants (Fig. 3E,F). This was in agreement with morphants not exhibiting head deformity. On the other hand, the ATG mo morphants exhibited a significantly higher incidence of developmental delay (Fig. 3A) and were significantly smaller in size (Figs 3D, S5B) compared to the control and E2I2 mo morphants at 2 dpf. The ATG mo morphants also exhibited significantly higher incidence of body axis abnormality than the control or E2I2 mo morphants (Fig. 3B). The incidence of heart abnormality was similar between the ATG mo morphants and control, but was threefold higher in E2I2 mo morphants compared to the control (Fig. 3C), suggesting that the phenotypes observed in R80S homozygous mutant fish are due to the loss-of-function effect of ESCO2. The phenotypes of ATG mo morphants and E2I2 mo morphants were different. The maternal and embryonic *ESCO2* are targets of ATG mo, and E2I2 mo may inhibit *ESCO2* after midblastula transition. Therefore, the difference of phenotype is attributable to the difference of timing for inhibition. Lastly, we crossed mutants (F4) of the original strain from the southern population, K-Cab, with another strain from the northern population, K-Kaga. The homozygous mutants ($ESCO2^{R80S/R80S}$) of the offspring (F′2) showed similar head deformities and developmental arrest by 2 dpf. Taken together, these results

demonstrate that R80S mutation is a loss-of-function mutation and is responsible for the developmental abnormality and the embryonic death.

Cytological abnormality in ESCO2 *mutant medaka*

Premature centromere separation (PCS) is caused by loss of ESCO2 and is diagnostic of RBS/SC (Schüle *et al.* 2005; Vega *et al.* 2005, 2010; Gordillo *et al.* 2008). To examine whether PCS is observed in R80S mutant medaka, we performed chromosomal analysis of 2-dpf embryos. Mutants showed a significant increase in the chromosomal abnormalities, including aneuploidy, chromosomal hyper-condensation and PCS (Fig. 4A, Table 2). Particularly, chromosomal hyper-condensation and PCS were observed in 39.6% and 6.6% of mutant cells, but only in 4.5% and 0.1% of WT, respectively. Thus, chromosomal abnormalities were observed in mutants similar to that in the *Eco1* mutant of yeast (Skibbens *et al.* 1999), with knocking down of *ESCO2* of HeLa cells (Hou & Zou 2005) and RBS/SC (Vega *et al.* 2005). The chromosomal hyper-condensation may be due to high sensitivity to colchicine in R80S mutants.

We monitored cells in the S-phase (Fig. 4B) and M-phase (Fig. 4C) with BrdU incorporation and an antibody to phosphorylated histone H3, respectively. Morphological differences between WT and mutant embryos were evident in the proliferative zone of the optic tectum, prospective corpus cerebelli, rhombic lips, pectoral fin buds and neural tube. In WT embryos, the proliferative cells were distinguishable and arranged in order. In contrast, the proliferative cells of mutants were widely distributed and out of order. The number of cells in the S- and M-phase tended to be slightly increased in mutants compared to WT embryos.

Next, we attempted cell cycle analysis by flow cytometry (Fig. 4D). In WT embryos, nuclei peaked at 2N DNA (corresponding to cells in the G1-phase), while a small fraction of cells were distributed between 2N and 4N DNA (S-phase), and at 4N DNA (G2/M-phase). Only 9.5% of cells were in the sub-G1 proportion. In contrast, mutant nuclei showed a marked increase in the sub-G1 population (41.2%) at the expense of cells in the G1-phase. Although a clear aneuploidy peak and enrichment of S and G2/M cells were not observed, S and G2/M cells slightly increased in mutants. To confirm the existence of apoptotic cells, we performed a TUNEL assay. In mutant embryos, a large number of cells underwent apoptosis throughout the body, while only a limited number of cells were TUNEL-positive in WT embryos (Fig. 4E). These results suggest that the R80S mutation of ESCO2 induces various chromosomal abnormalities including PCS and aneuploidy during cell division, and that the resulting apoptosis may cause developmental delay and eventual embryonic lethality.

Reduction of marker gene expression in ESCO2 *mutant medaka*

Because R80S mutant embryos showed morphological abnormalities, we analyzed the expression patterns of several marker genes, namely, *bf1*, *foxA2*, *iro3*, *krox20*, *notch1a*, *otx1* and *pax6*, as neural development and notochord markers, and *lfng* and *myf5* as somite markers using whole-mount *in situ* hybridization. The gene expression of almost all markers was downregulated and delayed in R80S mutants (Figs 5, S6). The expression of *pax6*, for example, in the eyes, was reduced in mutant embryos compared to WT ones at 2.0 dpf (Fig. 5A). However, when *pax6* expression in 2.0-dpf mutants was compared to 1.0-dpf WT, no significant differences were observed in the zona limitans intrathalamica. Similarly, the gene expression levels of *bf1*, *foxA2*, *iro3* and *lfng* in mutants at 2.0 dpf were similar to those in WT embryos at 1.0 dpf (Fig. S6). The *otx1* and *krox20* expression in 2.0-dpf mutants were similar to 1.5-dpf WT embryos (Fig. S6). Thus, the differences in expression were attributable to developmental retardation in mutants. The expression of *myf5* in mutants resembled 1.0-dpf and 2.0-dpf WT embryos (Fig. 5B). In contrast, strong reduction in *notch1a* expression was observed in mutants at 2.0 dpf (Fig. 5C,D). Because *notch1a* was expressed in WT embryos at 1.0–2.0 dpf, we speculate that this downregulation was not attributable to developmental retardation.

To confirm *notch1a* suppression in mutants, we quantified *notch1a*, *notch1b* (neurogenic markers [Lawson *et al.* 2002], Fig. 6A), and *ascl1a* and *ascl1b* (proneural markers, downstream targets of *notch1a* and *notch1b* in zebrafish [Allende & Weinberg 1994], Fig. 6B) mRNA of 2.0-dpf embryos by quantitative RT–PCR (qRT–PCR). We examined the genotype of all embryos prior to qRT–PCR and classified them into two groups: with and without morphological changes. Forty percent of the homozygous mutants were morphologically normal at 2.0 dpf. The neurogenic marker genes related to *notch* were dramatically suppressed in mutants exhibiting morphological abnormalities (Fig. 6A,B). Namely, the expression of *notch1a*, *notch1b*, *ascl1a* and *ascl1b* in mutants was suppressed by 41%, 50%, 9% and 8%, respectively, compared to the WT embryos. In contrast, no suppression of *notch1b* was observed in the morphologically normal mutants, while all the other neurogenic

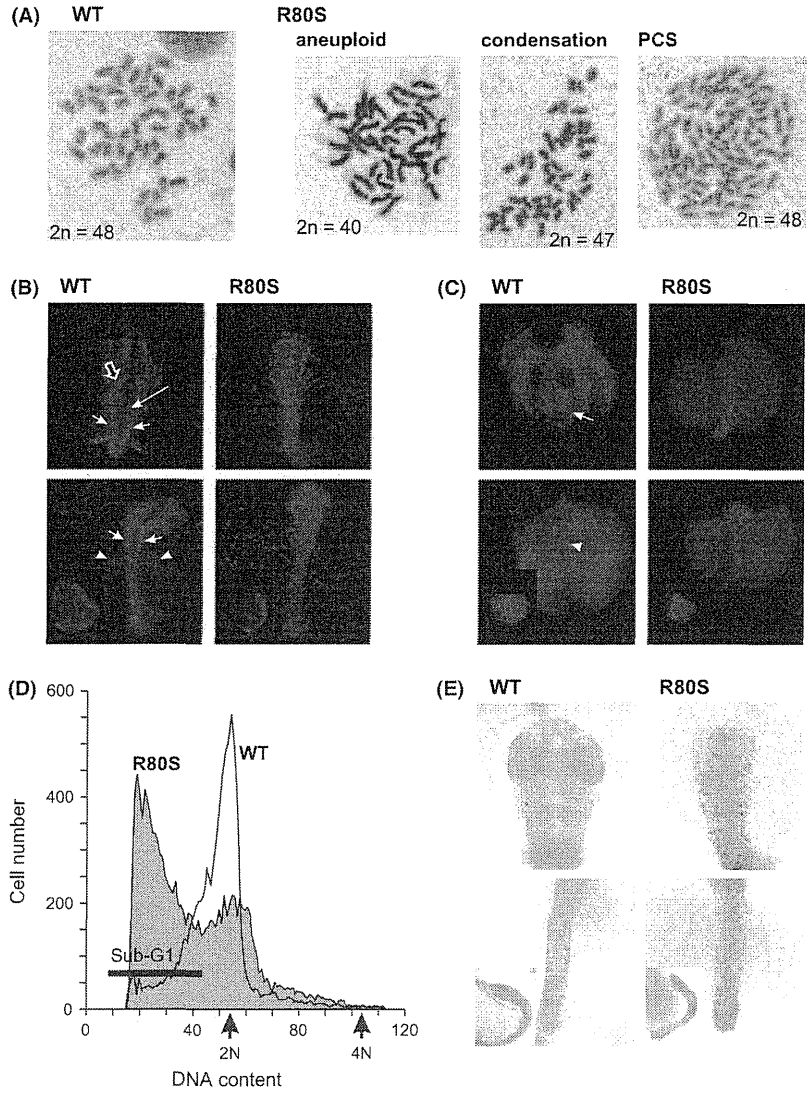

Fig. 4. Cytological abnormality of *ESCO2* mutant medaka. (A) Chromosomal analysis of wild-type (WT, leftmost) and R80S cells. Chromosomal preparation and Giemsa stain were applied to 2.0-days postfertilization (dpf) embryos. In R80S mutants, aneuploidy (shown as 2n = 40 versus 2n = 48 in WT), chromosomal hyper-condensation and premature centromere separation (PCS) were observed. (B) 5-bromodeoxyuridine (BrdU) labeling to detect cells in S-phase at 2.0 dpf. BrdU/Yamamoto solution (0.1%) was injected into the perivitelline space at 2.0 dpf. At 2 h after the injection, the embryos were fixed and immunohistochemically analyzed using anti-BrdU antibody. Top and bottom, dorsal view of the head and pectoral regions, respectively; inset in bottom panels, lateral view. BrdU labeling in the prospective corpus cerebelli (open arrow), rhombic lips (long arrow), the bilateral region of the midline (short arrows) and fin buds (arrowheads) was not detected in R80S mutants. (C) Anti-phosphorylated histone H3-labeling to detect cells in M-phase at 2.0 dpf. The embryos were fixed at 2.0 dpf and immunohistochemically analyzed by anti-phosphorylated histone H3 antibody. Top and bottom, dorsal view of the head and tail, respectively; inset of bottom panels, lateral view. The proliferating zone of the optic tectum and prospective corpus cerebelli (arrow) and the neural tube (arrowhead) was not immunoreactive in R80S mutant. (D) fluorescence-activated cell sorting (FACS) analysis of WT (open) and R80S (shaded) nuclei. The 2.0-dpf embryos were subjected to propidium iodide staining and FACS analysis. Note: the large proportion of R80S nuclei in sub-G1. (E) Terminal deoxynucleotidyl transferase-mediated dUTP nick end labeling assay indicates apoptotic cells throughout the whole body of R80S mutants. Top and bottom, dorsal view of the head and tail, respectively; inset of bottom panels, lateral view.

markers were suppressed by approximately 50% (Fig. 6A,B). We speculate that suppression of *notch1b* expression may be due to gross developmental defects and that the downregulation of *notch1a* is specific to *ESCO2* mutation regardless of developmental delay. Because *ascl1a* and *ascl1b* are downstream of

Table 2. Chromosomal analysis of medaka R80S mutants†

Genotype	*n*	Aneuploidy (%)	Hyper-condensation (%)	PCS (%)	String-like (%)
Embryos‡					
ESCO2$^{WT/WT}$	21	42.9	23.8	0.0	0.0
ESCO2$^{R80S/R80S}$	21	76.2*	71.4**	28.6**	19.0*
Cells					
ESCO2$^{WT/WT}$	941	6.2	4.5	0.1	0.1
ESCO2$^{R80S/R80S}$	182	25.3***	39.6***	6.6***	02.7***

*$P < 0.05$; **$P < 0.01$; ***$P < 0.001$, respectively (χ^2-test). †R80S embryos (F'2) were derived by crossing R80S (F4) heterozygous mutants of original strain with wild-type fish of another strain K-Kaga. The 2.0-days post fertilization (dpf) embryos were examined. ‡Embryos with more than 10% of cells exhibiting abnormalities are regarded as abnormal embryos. PCS, premature centromere separation.

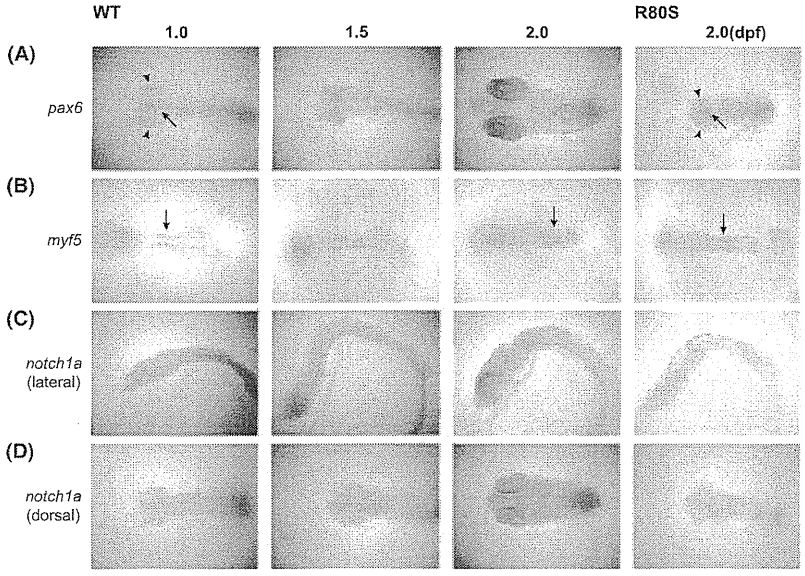

Fig. 5. Expression of marker gene in R80S (rightmost) and wild-type (WT) embryos. (A,B) Dorsal view of the *pax6* (A) and *myf5* (B) expression in the head and tail region, respectively. Expression of *pax6* in optic vesicles (arrowheads) is unclear in R80S mutant, but the expression in the zona limitans intrathalamica (arrows) is evident in both WT and R80S mutants. Expression of *myf5* (arrows) in R80S embryo resembles 1.0- and 2.0-day postfertilization (dpf) WT embryos. Lateral (C) and dorsal (D) view of the *notch1a* expression. Note: *notch1a* expression disappears in R80S mutant.

both *notch1a* and *notch1b*, the reduction of *ascl1a* and *ascl1b* may be more pronounced in morphologically abnormal mutants.

Next, we examined *GATA-1* and *notch3* (vascular differentiation markers in zebrafish [Lawson *et al.* 2001, 2002], Fig. 6C) because the heart was malformed in mutants. They were suppressed by 57% and 30%, respectively, in mutants with morphological abnormalities. In mutants with normal morphology, no significant reduction in *GATA-1* was observed (Fig. 6C), suggesting that *GATA-1* suppression may accompany general developmental delay, as is the case with *notch1b*. To confirm these data, we investigated the gene expression in morphants. We used the ATG mo and 5mis mo (as control), because ATG mo inhibits maternal and embryonic *ESCO2*. The ATG mo morphants showed suppression of *notch1a* (by 67%), *notch1b* (66%) and *notch3* (71%) (Fig. 6D,E). Downregulation of *notch1b* may be attributable to the developmental delay in ATG mo morphants (Fig. 3A). Thus, *ESCO2* mutation causes downregulation of *notch1a* and *notch3*. In summary, these data suggest that ESCO2 may play a role in embryogenesis through upregulation of critical genes such as *notch1a* and *notch3*.

Discussion

Establishment of RBS/SC model medaka

We established a medaka model of RBS/SC using the TILLING method and characterized it using a reverse

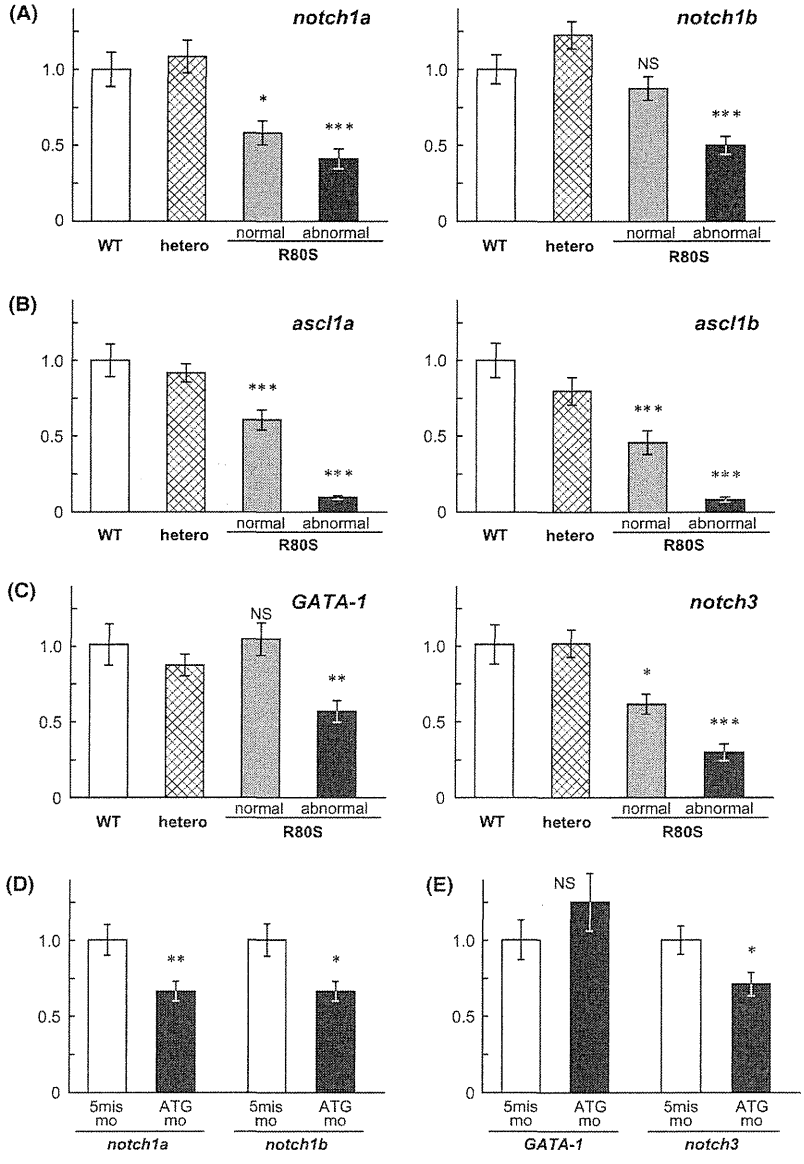

Fig. 6. Suppression of the expression of several genes in R80S embryos (A–C) and *ESCO2*-knockdown morphants (D,E). The expression of neurogenesis markers, *notch1a* and *notch1b* (A), neural progenitor markers, *ascl1a* and *ascl1b* (B) and vascular differentiation markers, *GATA-1* and *notch3* (C) in wild-type (WT), heterozygous (*ESCO2*$^{R80S/WT}$, hetero) and homozygous (*ESCO2*$^{R80S/R80S}$, R80S) mutants (2.0 days postfertilization [dpf]) was investigated by quantitative reverse transcription polymerase chain reaction. Normal and abnormal indicate apparently normal mutants and developmentally abnormal mutants, respectively. The expression of *notch1a* and *notch1b* (D) and *GATA-1* and *notch3* (E) in morphants (2.0 dpf) with the injection of 5mis mo (control) or ATG mo was examined. NS, *, ** and *** indicate $P \geq 0.05$, $P < 0.05$, $P < 0.01$ and $P < 0.001$, respectively, compared to WT or control embryos; ANOVA and Tukey's test, $n = 13$–14 (A–C); Student's *t*-test, $n = 13$ (D,E).

genetic approach. Morpholino antisense oligonucleotide is a very useful tool when using medaka or zebrafish as an animal model to efficiently reduce the expression of a gene of interest. However, it is sometimes difficult to ascertain the cause–effect relationship because morpholinos are often complicated by off-target effect. It should be especially difficult to analyze the morphants when the phenotypes vary as in RBS/SC. The mutant has a great advantage over morphants in that the gene alteration is fixed in the genome and the phenotypes can be analyzed in the uniform genetic background. Compared to other classical gene disruption methods such as homologous recombination and transposon/retrovirus insertion, TILLING has the great advantage of missense mutant recovery. Amino acid (a.a.) substitutions reveal the unexpected role of a protein, which cannot be obtained by knockout (KO) and knockdown methods. Missense mutants are particularly useful in the analysis of essential genes because simple disruption of the gene would cause lethality at the cellular or animal level. To our knowledge, *ESCO2*-KO mice have not been reported to date. Fish such as medaka are suited to investigation of the gene function during embryonic development as they develop *ex vivo*. The development of organs in fish share common molecular pathways with mammals. The developmental abnormality and death during development can be closely monitored in fish while

many of the lethal phenotypes may be overlooked in humans. Taken together, our system by using medaka could provide a powerful tool for investigating unidentified missense mutations in autosomal recessive disorders *in vivo*, even in embryonic lethal mutants.

The R80S mutant was created by ethyl nitroso urea (ENU) mutagenesis, which randomly introduces point mutations throughout the genome. In order to examine whether the observed phenotype was related to the R80S mutation, and to exclude the possibility that it was not derived from other mutation(s), we took two approaches: *in vivo* morpholino injections into the fertilized medaka eggs and linebreeding. The *ESCO2* morphants exhibited developmental abnormality and reduction of *notch1a* and *notch3* expression similar to that observed in the mutants. Moreover, the developmental and cytological abnormalities observed in mutants with a K-Cab (southern population) genetic background could be transferred to K-Kaga (northern population) genetic background by crossing original mutants with WT K-Kaga. Therefore, we suggest that the R80S mutation is responsible for the observed phenotypes.

Clinical feature in RBS/SC model medaka

The variety of phenotypes among individuals and the lack of a clear correlation between genotype and phenotype are some of the clinical features of RBS/SC. It has been shown that the same mutation results in different phenotypes in RBS/SC (Schüle *et al.* 2005; Vega *et al.* 2005, 2010; Gordillo *et al.* 2008). Recently, Mönnich *et al.* (2011) demonstrated that *ESCO2*-KD zebrafish showed craniofacial and fin abnormality. We summarized the phenotype of RBS/SC, R80S mutants, medaka *ESCO2* morphants (present study) and zebrafish *ESCO2* morphants (Mönnich *et al.* 2011) (Table 3). We also observed phenotypic diversity in our mutant medaka: craniofacial abnormalities, cardiac defect, growth retardation and PCS. RBS/SC is characterized by craniofacial abnormalities including bilateral cleft lip and/or palate, micrognathia, hypertelorism, exophthalmos, downslanting palpebral fissures, malar hypoplasia, hypoplastic nasal alae and ear malformation (Gordillo *et al.* 2006). R80S mutants exhibited a severe phenotype in the head region and were deficient in all head elements except for the eyes, even which showed developmental delay and incorrect structure. Thus, the morphological phenotype of the R80S mutant was very similar to RBS/SC and zebrafish *ESCO2* morphants except for limb abnormalities. The upper and lower limbs of humans and the pectoral and pelvic fins of medaka are evolutionarily derived from the same origins (Hinchliffe 2002). However, long bone growth in the stylopod and zeugopod is absent in the fins. Moreover, the fins have no part that is homologous to the autopod, which constitutes the distal part of mammalian limbs (Hinchliffe 2002). Therefore, phocomelia, long bone hypoplasia, ectrodactylia and brachydactylia cannot be detected in fish. In zebrafish *ESCO2* morphants, shorter and smaller fins were observed (Mönnich *et al.* 2011). Our R80S

Table 3. Summary of phenotypes of Roberts syndrome/SC phocomelia (RBS/SC) and medaka and zebrafish models

RBS/SC (human)	R80S mutants (medaka)	Morphants (medaka)	Morphants[†] (zebrafish)
Autosomal recessive	Autosomal recessive		
Intra uterine fetal death	Embryonic lethal	Survive	Embryonic lethal
Pre- and postnatal growth retardation	Developmental delay	Developmental delay	
	Small size	Small size	Small size
	Body axis abnormality	Body axis abnormality	Body axis abnormality
Craniofacial abnormality			
Microcephaly	Microcephaly	Normal	Smaller heads
Hyper telorism	Smaller and abnormal eye	Normal	Smaller eye
Hypoplastic nasal alae	Lack of nasal part	Normal	ND
Malar hypoplasia	Cartilage defect	ND	ND
Cleft lip and palate	Lack of mouth part	Normal	Lack of jaw
Limb abnormality			
Phocomelia	ND	ND	ND
Ulnar defects	ND	ND	ND
Radial defects	ND	ND	ND
Thumb defects	Normal (delayed)	Normal	Shorter and smaller fin
Renal abnormality	ND	ND	ND
Heart defect	Heart malformation	Heart malformation	Cardiac edema
Mental retardation	ND	ND	ND
Premature centromere separation	Premature centomere separation	ND	ND

[†]After Mönnich *et al.* 2011. ND, not determined.

mutants had normal pectoral fins. However, some of them exhibited developmental delay. Therefore, shorter and smaller fins of zebrafish morphants may correspond to the mutant fins developmentally delay. Medaka *ESCO2* morphants also had normal pectoral fins. The effect of morpholino was weaker in medaka than in zebrafish. This may be due to the time frame of morpholino action as medaka develops much more slowly than zebrafish and the effect of morpholino may be reduced by the time these organs are formed.

R80S mutants also exhibited developmental arrest by 2 dpf with incomplete penetrance (Table 1). Most of the escapers exhibited heart malformation and/or body axis abnormalities. This may be pertinent to the phenotypic variation observed in humans. Concerning congenital cardiac abnormality, atrial septal defect, ventricular septal defect and patent ducts arteriosus were reported (Gordillo *et al.* 2006). The escapers of R80S mutant and some of *ESCO2* morphants showed looping defect. Disturbance in cardiac looping is thought to cause congenital cardiac malformations (Männer 2009).

ESCO2-KD zebrafish showed cell cycle arrest and apoptosis with caspase activation (Mönnich *et al.* 2011). In R80S mutant of medaka, we could not clearly detect significant cell cycle arrest. This disagreement may be attributable to the difference of species or to the difference of knockdown (zebrafish) and missense mutant (medaka). We also detected apoptosis throughout the body in R80S mutants. This apoptosis may be associated with caspase activation, as in zebrafish. Moreover, microarray analysis revealed the gene regulated by ESCO2 in zebrafish and some gene regulation overlaps with cohesin-dependent transcription (Rhodes *et al.* 2010; Mönnich *et al.* 2011).

R80S mutation is responsible for embryonic death, and deficiency of Eco1 in yeast causes cellular lethality. On the contrary, RBS/SC patients can give birth. It was reported that the related molecule, ESCO1 in humans, and suggested that ESCO1 and ESCO2, play distinct roles in cell cycle progression (Hou & Zou 2005). Although ESCO1 and ESCO2 acetylate SMC3, the knocking down of *ESCO1* is more effective on the SMC acetylation than that of *ESCO2* in humans (Zhang *et al.* 2008). The different effect of functional deficiency in ESCO2 between RBS/SC patients and R80S mutants may be explainable by the difference of functionalization of ESCO1 and ESCO2. The function of ESCO1 in medaka needs to be elucidated. On the other hand, the mutant medaka showed more severe phenotypes than RBS/SC and morphants of medaka and zebrafish. Only mutant medaka is embryonically lethal. RBS/SC patients are rare and RBS/SC is characterized by intrauterine fetal death. A few R80S mutants can live up to adult fish. Thus, RBS/SC patients may be escapers as in R80S mutants. The escapers of R80S mutants will be analyzed in a future study.

R80S mutation

We have found that the mutation in the conserved amino acid (a.a.) in the N-terminal portion of ESCO2, R80 (in human K), disrupts the establishment of cohesion function of ESCO2, demonstrating the importance of this previously undescribed region of this protein. This is the first case in which a missense mutation outside the acetyltransferase domain causes the loss-of function phenotype. The region (73–84 a.a.) including R80 is well conserved from fish to humans, although the mutation in this region has not been reported in RBS/SC. ECO1 lacks this region. Although Eso1 (Tanaka *et al.* 2010), budding yeast homologue, deco (Williams *et al.* 2003), *Drosophila* homologue and ESCO1 (Hou & Zou 2005) of humans contain extradomain at the N-termius, no motif or similarity have been found in the N-terminal portion of ESCO2. The molecular function of this conserved region is of special interest.

Variety of clinical features in RBS/SC

The *ESCO2* expression in the proliferating region and the chromosomal phenotype, namely, PCS, caused by the R80S mutation indicate that ESCO2 plays an important role in cell division in medaka. In other species, ESCO2 functions in the establishment of sister chromatid cohesion via acetylation of the cohesin complex (Rolef Ben-Shahar *et al.* 2008; Unal *et al.* 2008; Zhang *et al.* 2008). Therefore, the R80S mutation of ESCO2 may cause a reduction of cohesin complex acetylation, resulting in an anti-establishment state in sister chromatid cohesion during S-phase similar to that in other species including humans. On the other hand, RBC/SC has a variety of clinical features (Schüle *et al.* 2005; Vega *et al.* 2005, 2010; Gordillo *et al.* 2008). The same mutation of ESCO2 causes different phenotypes. R80S mutants also have a variety of clinical phenotypes. Pathological features in the establishment of sister chromatid cohesion are attributable to a lack of ESCO2 function in cell division. However, this is not sufficient to explain the variety in the clinical features. The cohesin complex, the target of ESCO2, causes Cornelia de Lange syndrome (CdLS) (OMIM 122470, 300590 and 610759). CdLS also has a variety of clinical features (Dorsett 2007; Liu & Krantz 2009). The clinical features of CdLS are distinct from RBS/SC, but with some overlap (Liu & Krantz 2009). Recently, cohesion-mediated gene regulation was

demonstrated in *Drosophila*, zebrafish, mice and humans. Homeobox gene expression is required for Nipped-B, a cohesin regulator in *Drosophila* (Dorsett 2009). The gene expressions of *runx1* and *runx3* (transcription factors) are required for Rad21 and Smc3 (components of the cohesin complex) in zebrafish (Horsfield *et al.* 2007). Genome-wide chromatin immunoprecipitation experiments in human and mouse cells have revealed co-localization of cohesin and CTCF, a zinc-finger protein with enhancer blocking and barrier activities (Parelho *et al.* 2008; Stedman *et al.* 2008; Wendt *et al.* 2008). CTCF is thought to have a potential function in directly regulating gene transcription both positively and negatively (Ishihara *et al.* 2006; Chernukhin *et al.* 2007). ESCO2 functions in establishment of sister chromatid cohesion by acetylation of the cohesin complex. Therefore, mutation of ESCO2 may cause lack of functional cohesin. Consequently, it is suggested that mutation of ESCO2 affects the expression of several genes. In this study, we demonstrated that R80S mutation actually suppresses *notch1a*, its downstream genes and *notch3* expression. Downregulation of *notch1a* and its downstream gene expression result from the mutation of the cohesin component in zebrafish (Horsfield *et al.* 2007). Therefore, we propose that the neural and heart malformations may involve downregulation of these genes in R80S mutant medaka and RBS/SC. The clinical feature of cardiac defects in R80S mutants is similar to the medaka knocking-down of congenital heart disease 5 (*mCHD5*) gene function (Murata *et al.* 2009). *Notch3* suppressed in ESCO2 R80S mutant may be involved in *mCHD5* expression. Recently, cohesin-independent regulation of gene expression by Eco1 was reported (Choi *et al.* 2010). Eco1 suppresses transcription via association with histone demethylase, LSD1, to convert chromatin to an inactive state. Thus, ESCO2 regulates the expression of several genes. Research on the genes regulated by ESCO2 is an interesting area for further study. The functional analyses of ESCO2 have only been performed at cellular level so far. This mutant medaka enables analysis at a whole-body level, particularly, in the early embryonic development. The mechanisms producing the pathological variety of RBS/SC will be elucidated.

In conclusion, we isolated *ESCO2* mutant medaka from the TILLING library and characterized it using a reverse genetic approach. The *ESCO2*$^{R80S/R80S}$ homozygous mutants had phenotypic features reminiscent of RBS/SC. From the gene expression analysis, some gene expression was downregulated in mutants. Thus *ESCO2* mutant medaka is the animal model for RBS/SC and a valuable resource for future research.

Acknowledgments

We thank A. Koide, Y. Nakura, RIMCH, and Professor T. Hashimoto-Tamaoki, Hyogo College of Medicine, for technical support, and K. Mimura, F. Namba, M. Nishihara, K. Ohnishi and M. Nozaki, RIMCH for rearing of medaka strains. We also thank Dr K. Inohaya of Tokyo Institute of Technology and Dr S. Yasumasu of Sophia University for kindly providing the molecular markers. We thank National BioResource Project (NBRP) Medaka for the kindly gifted K-Kaga strain, Dr M. Seiki and Professor H. Kondoh, SORST, Kondoh Research Team, JST, for kindly providing the Kyoto-Cab strain, and Dr K. Naruse of NBRP Medaka for helpful information and suggestion. This work was supported in part by Grants-in-Aid from the Ministry of Health, Labor and Welfare, Japan; the Ministry of Education, Culture, Sports, Science and Technology (MEXT), Japan; and Osaka Research Society for Pediatric Infectious Diseases, Osaka, Japan.

References

Aizawa, K., Shimada, A., Naruse, K., Mitani, H. & Shima, A. 2003. The medaka midblastula transition as revealed by the expression of the paternal genome. *Gene Expr. Patterns* **3**, 43–47.

Allende, M. L. & Weinberg, E. S. 1994. The expression pattern of two zebrafish achaete-scute homolog (ash) genes is alterd in the embryonic brain of the cyclops mutant. *Dev. Biol.* **166**, 509–530.

Candal, E., Alunni, A., Thermes, V., Jamen, F., Joly, J.-S. & Bourrat, F. 2007. *Ol-insm1b*, a SNAG family transcription factor involved in cell cycle arrest during medaka development. *Dev. Biol.* **309**, 1–17.

Chernukhin, I., Shamsuddin, S., Kang, S. Y., Bergström, R., Kwon, Y.-W., Yu, W. Q., Whitehead, J., Mukhopadhyay, R., Docquier, F., Farrar, D., Morrison, I., Vigneron, M., Wu, S. Y., Chiang, C. M., Loukinov, D., Lobanenkov, V., Ohlsson, R. & Klenova, E. 2007. CTCF interacts with and recruits the largest subunit of RNA polymerase II to CTCF target sites genome-wide. *Mol. Cell. Biol.* **27**, 1631–1648.

Choi, H. K., Kim, B.-J., Seo, J.-H., Kang, J.-S., Cho, H. & Kim, S.-T. 2010. Cohesion establishment factor, Eco1 represses transcription via association with histone demethylase, LSD1. *Biochem. Biophys. Res. Commun.* **394**, 1063–1068.

Dorsett, D. 2007. Roles of the sister chromatid cohesion apparatus in gene expression, development, and human syndromes. *Chromosoma* **116**, 1–13.

Dorsett, D. 2009. Cohesin, gene expression and development: lessons from *Drosophila*. *Chromosome Res.* **17**, 185–200.

Furutani-Seiki, M., Sasado, T., Morinaga, C., Suwa, H., Niwa, K., Yoda, H., Deguchi, T., Hirose, Y., Yasuoka, A., Henrich, T., Watanabe, T., Iwanami, N., Kitagawa, D., Saito, K., Asaka, S., Osakada, M., Kunimatsu, S., Momoi, A., Elmasri, H., Winkler, C., Ramialison, M., Loosli, F., Quiring, R., Carl, M., Grabher, C., Winkler, S., Del Bene, F., Shinomiya, A., Kota, Y., Yamanaka, T., Okamoto, Y., Takahashi, K., Todo, T., Abe, K., Takahama, Y., Tanaka, M., Mitani, H., Katada, T., Nishina, H., Nakajima, N., Wittbrodt, J. & Kondoh, H. 2004.

A systematic genome-wide screen for mutations affecting organogenesis in Medaka *Oryzias latipes*. *Mech. Dev.* **121**, 647–658.

Gordillo, M., Vega, H., Trainer, A. H., Hou, F., Sakai, N., Luque, R., Kayserili, H., Basaran, S., Skovby, F., Hennekam, R. C. M., Uzielli, M. L., Schnur, R. E., Manouvrier, S., Chang, S., Blair, E., Hurst, J. A., Forzano, F., Meins, M., Simola, K. O., Raas-Rothschild, A., Schultz, R. A., McDaniel, L. D., Ozono, K., Inui, K., Zou, H. & Jabs, E. W. 2008. The molecular mechanism underlying Roberts syndrome involves loss of ESCO2 acetyltransferase activity. *Hum. Mol. Genet.* **17**, 2172–2180.

Gordillo, M., Vega, H. & Jabs, E. W. 2006. Roberts syndrome. In: *GeneReviews* (eds Pagon RA, Bird TD, Dolan CR, Stephens K & Adam MP). University of Washington, Seattle, WA. 1993.

Hinchliffe, J. R. 2002. Develomental basis of limb evolution. *Int. J. Dev. Biol.* **46**, 835–845.

Horsfield, J. A., Anagnostou, S. H., Hu, J. K.-H., Cho, K. H. Y., Geisler, R., Kieschke, G., Crosier, K. E. & Crosier, P. S. 2007. Cohesin-dependent regulation of *Runx* genes. *Development* **134**, 2639–2649.

Hou, F. & Zou, H. 2005. Two human orthologues of Eco1/Ctf7 acetyltransferases are both required for proper sister-chromatid cohesion. *Mol. Biol. Cell* **16**, 3908–3918.

Iijima, N. & Yokoyama, T. 2007. Apoptosis in the medaka embryo in the early developmental stage. *Acta Histochem. Cytochem.* **40**, 1–7.

Ishihara, K., Oshimura, M. & Nakao, M. 2006. CTCF-dependent chromatin insulator is linked to epigenetic remodeling. *Mol. Cell* **23**, 733–742.

Ishikawa, Y. 2000. Medakafish as a model system for vertebrate developmental genetics. *BioEssays* **22**, 487–495.

Ivanov, D., Schleiffer, A., Eisenhaber, F., Mechtler, K., Haering, C. H. & Nasmyth, K. 2001. Eco1 is a novel acetyltransferase that can acetylate proteins involved in cohesion. *Curr. Biol.* **12**, 323–328.

Iwamatsu, T. 1994. Stages of normal development in the medaka *Oryzias latipes*. *Zool. Sci.* **11**, 825–839.

Kage, T., Takeda, H., Yasuda, T., Maruyama, K., Yamamoto, N., Yohimoto, M., Araki, K., Inohaya, K., Okamoto, H., Yasumasu, S., Watanabe, K., Ito, H. & Ishikawa, Y. 2004. Morphogenesis and regionalization of the medaka embryonic brain. *J. Comp. Neurol.* **476**, 219–239.

Kasahara, M., Naruse, K., Sasaki, S., Nakatani, Y., Qu, W., Ahsan, B., Yamada, T., Nagayasu, Y., Doi, K., Kasai, Y., Jindo, T., Kobayashi, D., Shimada, A., Toyoda, A., Kuroki, Y., Fujiyama, A., Sasaki, T., Shimizu, A., Asakawa, S., Shimizu, N., Hashimoto, S., Yang, J., Lee, Y., Matsushima, K., Sugano, S., Sakaizumi, M., Narita, T., Ohishi, K., Haga, S., Ohta, F., Nomoto, H., Nogata, K., Morishita, T., Endo, T., Shin-I, T., Takeda, H., Morishita, S. & Kohara, Y. 2007. The medaka draft genome and insights into vertebrate genome evolution. *Nature* **447**, 714–719.

Lawson, N. D., Scheer, N., Pham, V. N., Kim, C.-H., Chitins, A. B., Campos-Ortega, J. & Westein, B. M. 2001. Notch signaling is required for arterial-venous differentitation during embryonic vascular development. *Development* **128**, 3675–3683.

Lawson, N. D., Vogel, A. M. & Weinstein, B. M. 2002. *Sonic hedgehog* and *vascular endothelial growth factor* act upstream of the notch pathway during arterial endothelial differentiation. *Dev. Cell* **3**, 127–136.

Liu, J. & Krantz, I. D. 2009. Cornelia de Lange syndrome, cohesin, and beyond. *Clin. Genet.* **76**, 303–314.

Männer, J. 2009. The anatomy of cardiac looping: a step towards the understanding of the morphogenesis of several forms of congenital cardiac malformations. *Clin. Anat.* **22**, 21–35.

Moldovan, G. L., Pfander, B. & Jentsch, S. 2006. PCNA controls establishment of sister chromatid cohesion during S phase. *Mol. Cell* **23**, 723–732.

Mönnich, M., Kuriger, Z., Print, C. G. & Horsfield, J. A. 2011. A zebrafish model of Roberts syndrome reveals that esco2 depletion interferes with development by disrupting the cell cycle. *PLoS ONE* **6**, e20051.

Murata, K., Degmetich, S., Kinoshita, M. & Shimada, E. 2009. Expression of the congenital heart disease 5/tryptophan rich basic protein homologue gene during heart development in medaka fish, *Oryzias latipes*. *Dev. Growth Differ.* **51**, 95–107.

Nguyen, V., Deschet, K., Henrich, T., Godet, E., Joly, J.-S., Wittbridt, J., Chourrout, D. & Bourrat, F. 1999. Morphogenesis of the optic tectum in the medaka (*Oryzias latipes*): a morphological and molecular study with special emphasis on cell proliferation. *J. Comp. Neurol.* **413**, 385–404.

Nishihara, M., Yamada, M., Nozaki, M., Nakahira, K. & Yanagihara, I. 2010. Transcriptional regulation of the human establishment of cohesion 1 homolog 2 gene. *Biochem. Biophys. Res. Commun.* **393**, 111–117.

Onn, I., Guacci, V. & Koshland, D. E. 2009. The zinc finger of Eco1 enhances its acetyltransferase activity during sister chromatid cohesion. *Nucleic Acids Res.* **37**, 6126–6134.

Parelho, V., Hadjur, S., Spivakov, M., Leleu, M., Sauer, S., Gregson, H. C., Jarmuz, A., Canzonetta, C., Webster, Z., Nesterova, T., Cobb, B. S., Yokomori, K., Dillon, N., Aragon, L., Fisher, A. G. & Merkenschlager, M. 2008. Cohesins functionally associate with CTCF on mammalian chromosome arms. *Cell* **132**, 422–433.

Rembold, M., Lahiri, K., Foulkes, N. S. & Wittbrodt, J. 2006. Transgenesis in fish: efficient selection of transgenic fish by co-injection with a fluorescent reporter construct. *Nat. Protoc.* **1**, 1133–1139.

Rhodes, J. M., Bentley, F. K., Print, C. G., Dorsett, D., Misulovin, Z., Dickinson, E. J., Crosier, K. E., Crosier, P. S. & Horsfield, J. A. 2010. Positive regulation of c-*Myc* by cohesin is direct, and evolutionarily conserved. *Dev. Biol.* **344**, 637–649.

Rolef Ben-Shahar, T., Heeger, S., Lehane, C., East, P., Flynn, H., Skehel, M. & Uhlmann, F. 2008. Eco1-dependent cohesin acetylation during establishment of sister chromatid cohesion. *Science* **321**, 563–566.

Schüle, B., Oviedo, A., Johnston, K., Pai, S. & Francke, U. 2005. Inactivating mutations in ESCO2 cause SC phocomelia and Roberts syndrome: no phenotype-genotype correlation. *Am. J. Hum. Genet.* **77**, 1117–1128.

Skibbens, R. V., Corson, L. B., Koshland, D. & Hieter, P. 1999. Ctf7p is essential for sister chromatid cohesion and links mitotic chromosome structure to the DNA replication machinery. *Genes Dev.* **13**, 307–319.

Stedman, W., Kang, H., Lin, S., Kissil, J. L., Bartolomei, M. S. & Lieberman, P. M. 2008. Cohesins localize with CTCF at the KSHV latency control region and at cellular c-myc and H19/Igf2 insulators. *EMBO J.* **27**, 654–666.

Tanaka, K., Yonekawa, T., Kawasaki, Y., Kai, M., Furuya, K., Iwasaki, M., Murakami, H., Yanagida, M. & Okayama, H. 2010. Fission yeast Eso1p is required for establishing sister chromatid cohesion during S phase. *Mol. Cell. Biol.* **20**, 3459–3469.

Taniguchi, Y., Takeda, S., Furutani-Seiki, M., Kamei, Y., Todo, T., Sasado, T., Deguchi, T., Kondoh, H., Mudde, J.,

Yamazoe, M., Hidaka, M., Mitani, H., Toyaoda, A., Sakaki, Y., Plasterk, R. H. & Cuppen, E. 2006. Generation of medaka gene knockout models by target-selected mutagenesis. *Genome Biol.* **7**, R116.

Terasaki, H., Murakami, R., Yasuhiko, Y., Shin-i, T., Kohara, Y., Saga, Y. & Takeda, H. 2006. Transgenic analysis of the medaka *mesp-b* enhancer in somitogenesis. *Dev. Growth Differ.* **48**, 153–168.

Terret, M. E., Sherwood, R., Rahman, S., Qin, J. & Jallepalli, P. V. 2009. Cohesin acetylation speeds the replication fork. *Nature* **462**, 231–234.

Unal, E., Heidinger-Pauli, J. M., Kim, W., Guacci, V., Onn, I., Gygi, S. P. & Koshland, D. E. 2008. A molecular determinant for the establishment of sister chromatid cohesion. *Science* **321**, 566–569.

Vega, H., Trainer, A. H., Gordillo, M., Crosier, M., Kayserili, H., Skovby, F., Giovannucci Uzielli, M. L., Schnur, R. E., Manouvrier, S., Blair, E., Hurst, J. A., Forzano, F., Meins, M., Simola, K. O. J., Raas-Rothschild, A., Hennekam, R. C. M. & Jabs, E. W. 2010. Phenotypic variability in 49 cases of ESCO2 mutations, including novel missense and codon deletion in the acetyltransferase domain, correlates with ESCO2 expression and established the clinical criteria for Roberts syndrome. *J. Med. Genet.* **47**, 30–37.

Vega, H., Waisfisz, Q., Gordillo, M., Sakai, N., Yanagihara, I., Yamada, M., van Gosliga, D., Kayserili, H., Xu, C., Ozono, K., Jabs, E. W., Inui, K. & Joenje, H. 2005. Roberts syndrome is caused by mutations in ESCO2, a human homolog of yeast ECO1 that is essential for the establishment of sister chromatid cohesion. *Nat. Genet.* **37**, 468–470.

Wendt, K. S., Yoshida, K., Itoh, T., Bando, M., Koch, B., Schirghuber, E., Tsutsumi, S., Nagae, G., Ishihara, K., Mishiro, T., Yahata, K., Imamoto, F., Aburatani, H., Nakao, M., Imamoto, N., Maeshima, K., Shirahige, K. & Peters, J. M. 2008. Cohesin mediates transcriptional insulation by CCCTC-binding factor. *Nature* **451**, 796–801.

Westerfield, M. 2000. *The Zebrafish Book. A Guide for the Laboratory Use of Zebrafish (Danio rerio)*, 4th edn. University of Oregon Press, Eugene, Oregon.

Whitfield, M. L., Sherlock, G., Saldanha, A. J., Murray, J. I., Ball, C. A., Alexander, K. E., Matese, J. C., Perou, C. M., Hurt, M. M., Brown, P. O. & Botstein, D. 2000. Identification of genes periodically expressed in the human cell cycle and their expression in tumors. *Mol. Biol. Cell* **13**, 1977–2000.

Williams, B. C., Garrett-Engele, C. M., Li, Z., Williams, E. V., Rosenman, E. D. & Goldberg, M. L. 2003. Two putative acetyltransferases, san and deco, are required for establishing sister chromatid cohesion in *Drosophila*. *Curr. Biol.* **13**, 2025–2036.

Yasutake, J., Ihohaya, K. & Kudo, A. 2004. *Twist* functions in vertebral column formation in medaka, *Oryzias latipes*. *Mech. Dev.* **121**, 883–894.

Zar, J. H. 2010. *Biostatistical Analysis*, 5th edn. Pearson Education Inc., Upper Saddle River, NJ.

Zhang, J., Shi, X., Li, Y., Kim, B.-J., Jia, J., Huang, Z., Yang, T., Fu, X., Jung, S. Y. & Wang, Y. 2008. Acetylation of Smc3 by Eco1 is required for S phase sister chromatid cohesion in both human and yeast. *Mol. Cell* **31**, 143–151.

Supporting Information

Additional Supporting Information may be found in the online version of this article:

Figure S1. Alignment of deduced amino acid sequences of ESCO2 in medaka (*Oryzias latipes*), human (*Homo sapiens*, accession no. NP_001017420), mouse (*Mus musculus*, accession no. NP_082315) and zebrafish (*Danio rerio*, accession no. Q5SPR8).

Figure S2. Expression of *ESCO2* in early development of medaka embryo.

Figure S3. Developmental profile of the expression alleles of *ESCO2*.

Figure S4. Construction of morpholinos.

Figure S5. Pectoral width of WT (empty bars) and R80S (solid bars) embryos (2.0 dpf, A), and morphants (2.0 dpf) with 300 nmol/L of 5mis mo (empty bars), ATG mo (solid bars) or E2I2 mo (shaded bars) injected just after fertilization (B). dpf, days postfertilization; WT, wild type.

Figure S6. Expression of marker gene in R80S (uppermost) and wild-type embryos.

Table S1. Primer using for cloning, genotyping and real-time polymerase chain reaction.

Please note: Wiley-Blackwell are not responsible for the content or functionality of any supporting materials supplied by the authors. Any queries (other than missing material) should be directed to the corresponding author for the article.

Role of DNA Methylation in the Regulation of Lipogenic Glycerol-3-Phosphate Acyltransferase 1 Gene Expression in the Mouse Neonatal Liver

Tatsuya Ehara,[1,2] Yasutomi Kamei,[1,3] Mayumi Takahashi,[1] Xunmei Yuan,[1] Sayaka Kanai,[1] Erina Tamura,[1] Miyako Tanaka,[1,3] Tomomi Yamazaki,[4] Shinji Miura,[4] Osamu Ezaki,[4] Takayoshi Suganami,[1] Masaki Okano,[5] and Yoshihiro Ogawa[1,6,7]

The liver is a major organ of lipid metabolism, which is markedly changed in response to physiological nutritional demand; however, the regulation of hepatic lipogenic gene expression in early life is largely unknown. In this study, we show that expression of glycerol-3-phosphate acyltransferase 1 (GPAT1; *Gpam*), a rate-limiting enzyme of triglyceride biosynthesis, is regulated in the mouse liver by DNA methylation, an epigenetic modification involved in the regulation of a diverse range of biological processes in mammals. In the neonatal liver, DNA methylation of the *Gpam* promoter, which is likely to be induced by Dnmt3b, inhibited recruitment of the lipogenic transcription factor sterol regulatory element–binding protein-1c (SREBP-1c), whereas in the adult, decreased DNA methylation resulted in active chromatin conformation, allowing recruitment of SREBP-1c. Maternal overnutrition causes decreased *Gpam* promoter methylation with increased GPAT1 expression and triglyceride content in the pup liver, suggesting that environmental factors such as nutritional conditions can affect DNA methylation in the liver. This study is the first detailed analysis of the DNA-methylation–dependent regulation of the triglyceride biosynthesis gene *Gpam*, thereby providing new insight into the molecular mechanism underlying the epigenetic regulation of metabolic genes and thus metabolic diseases. ***Diabetes* 61:2442–2450, 2012**

The liver is a major organ of lipid metabolism, which is physiologically changed during organ maturation (1,2). The rate of hepatic de novo lipogenesis (i.e., triglyceride [TG] biosynthesis) is very low during the suckling period, when fat intake is high from milk, but it rises with the onset of weaning, when glucose is used as a source of energy (1). Thus, hepatic gene expression may change markedly before and after weaning, which could be regulated in response to nutritional demand.

TG is the major storage form of energy in animals. TG biosynthesis begins with the acylation of glycerol-3-phosphate by glycerol-3-phosphate acyltransferase 1 (GPAT1; *Gpam*) to form lysophosphatidic acid; this is the rate-limiting step in the hepatic TG biosynthesis pathway (3). In the acylation process, fatty acids produced by stearoyl CoA desaturase 1 (SCD1; *Scd1*) and fatty acid synthase (FAS; *Fasn*) are used as acyl donors. Among the lipogenic enzymes, GPAT1 plays an important role in the regulation of hepatic TG biosynthesis (4,5). The lipogenic genes such as *Gpam*, *Scd1*, and *Fasn* are activated by sterol regulatory element–binding protein-1c (SREBP-1c), which is a transcription factor and master regulator of lipogenesis. Indeed, their promoter regions contain the SREBP-responsive elements (SREs) (6–8). Aberrant lipogenic gene regulation can contribute to fatty liver, which is associated with obesity, type 2 diabetes, and insulin resistance (9). However, the molecular mechanism involved in the regulation of lipogenic genes during early life remains largely unclear.

The methylation of cytosine residues in DNA is a major epigenetic modification, and its role is well studied in organ development and cell differentiation (10–12). In most instances, DNA methylation of the promoter regions causes suppression of gene expression (13). In mammals, three CpG DNA methyltransferases (Dnmt)—Dnmt1, Dnmt3a, and Dnmt3b—coordinately regulate DNA methylation in the genome. Dnmt1 promotes DNA methylation after DNA replication and plays a major role in the maintenance of methylation (14). Dnmt3a and Dnmt3b are required for the initiation of de novo DNA methylation (10).

DNA methylation may be affected by environmental factors, thereby regulating a variety of metabolic processes and diseases (15–18). Although the fetal and neonatal periods, which are highly plastic to environmental changes, should be under the epigenetic control, the role of DNA methylation in early life has not fully been addressed. This study is the first demonstration that the DNA methylation status of the *Gpam* promoter and its mRNA expression are inversely correlated during mouse liver maturation. This study highlights the role of DNA methylation in the regulation of lipogenic genes, thereby providing new insight into the molecular mechanism underlying epigenetic regulation of metabolic diseases.

RESEARCH DESIGN AND METHODS

Animals and the experiment with high-fat/high-sucrose diet–fed dams. Pregnant female C57BL/6 mice were obtained from Japan SLC (Hamamatsu, Japan). The mice were fed ad libitum a standard rodent chow, CRF1 (Charles River Japan, Tokyo, Japan). Offspring at the indicated ages were used for tissue

From the [1]Department of Molecular Medicine and Metabolism, Medical Research Institute, Tokyo Medical and Dental University, Tokyo, Japan; the [2]Functional Food Research Department, Food Science and Technology Institute, Morinaga Milk Industry Co., Ltd., Kanagawa, Japan; the [3]Department of Organ Network and Metabolism, Medical Research Institute, Tokyo Medical and Dental University, Tokyo, Japan; the [4]Nutritional Science Program, National Institute of Health and Nutrition, Tokyo, Japan; the [5]Laboratory for Mammalian Epigenetic Studies, Center for Developmental Biology, RIKEN, Kobe, Japan; the [6]Department of Molecular Endocrinology and Metabolism, Graduate School of Medical and Dental Sciences, Tokyo Medical and Dental University, Tokyo, Japan; and the [7]Global Center of Excellence Program, International Research Center for Molecular Science in Tooth and Bone Diseases, Medical Research Institute, Tokyo Medical and Dental University, Tokyo, Japan.

Corresponding author: Yoshihiro Ogawa, ogawa.mem@tmd.ac.jp.

Received 4 January 2012 and accepted 19 April 2012.

DOI: 10.2337/db11-1834

This article contains Supplementary Data online at http://diabetes.diabetesjournals.org/lookup/suppl/doi:10.2337/db11-1834/-/DC1.

T.E. and Y.K. contributed equally to this work.

sampling. They were weaned at 25 days of age and thereafter fed CRF1 throughout the experiment.

The experiment with high-fat/high-sucrose (HF/HS) diet–fed dams was performed as follows. Six-week-old male and female C57BL/6 mice (Japan SLC) were crossed, and pregnant dams were used. Two weeks before the beginning of mating and throughout the experiment, dams were fed ad libitum either CRF1 (standard) or HF/HS diet (D12079B; Research Diets, New Brunswick, NJ). Schematic experimental design is shown in Supplementary Fig. 1. Five-day-old offspring were used for analysis. All animal experiments were approved by Institutional Animal Care and Use Committee of Tokyo Medical and Dental University (approval identification number 0090041).

Quantitative real-time PCR analysis. Gene expression levels were measured as described (19). The primers used are shown in Supplementary Table 1.

Western blot analysis. The nuclear fraction of cell lysate was prepared using a ProteoJET Cytoplasmic and Nuclear Protein Extraction Kit (Fermentas, Glen Burnie, MD). Mitochondrial fraction of the liver was prepared as described (4). Western blot analysis was performed as described previously (19). Anti-GPAT1 (sc-161674; Santa Cruz Biotechnology, Santa Cruz, CA), anti-SCD1 (ab19862; Abcam, Cambridge, MA), anti-FAS (sc-48357; Santa Cruz Biotechnology), anti–SREBP-1 (ab3259; Abcam), anti-CoxIV (ab14774; Abcam), anti–α-tubulin (T9026; Sigma-Aldrich, St. Louis, MO), anti-Lamin a/c (sc-20681; Santa Cruz Biotechnology), anti-Dnmt3b (IMG184A; Imgenex, San Diego, CA), or histone H1 (sc-10806; Santa Cruz Biotechnology) was used as the primary antibody.

Bisulfite DNA methylation analysis. Sodium bisulfite treatment of genomic DNA was performed with a BisulFast DNA modification kit (Toyobo, Tokyo, Japan) according to the manufacturer's instructions. Sequential PCR amplification of the genes of interest was performed using specific primers (Supplementary Table 2). The PCR profile was as described in Supplementary Table 2. The amplified fragments were ligated into the vector pGEM-T-easy (Promega KK, Tokyo, Japan) and sequenced. At least 16 bacterial colonies were picked up per PCR amplification. A web-based tool, quantification tool for methylation analysis, was used for bisulfite sequencing analysis of CpG methylation (http://quma.cdb.riken.jp/) (20).

Quantification of DNA methylation of the *Gpam* promoter. DNA digestion with methylation-sensitive *Hpa*II and quantitative real-time PCR were performed as described previously (21), with the following primers: forward primer 5′-CCCTAAAACTGGCTCCGGA-3′ and reverse primer 5′-CAGCCAATCGAAAGCTTCAGA-3′. The forward primer contains the *Hpa*II site of *Gpam* promoter (underlined).

Primary culture of mouse hepatocytes. Primary hepatocytes were isolated as described previously (22,23).

Preparation of recombinant adenovirus. The full-length mouse Dnmt3b1 cDNA was subcloned into the pShuttle vector provided in the BD Adeno-X Expression System (BD Biosciences, Franklin Lakes, NJ). BD Adeno-X enhanced green fluorescent protein (GFP) was used as a control (Ad-GFP; BD Biosciences). Ad–SREBP-1c (active-nuclear form) (24) was kindly provided from Dr. Hitoshi Shimano (Tsukuba University). Each recombinant adenovirus (Ad-Dnmt3b, Ad-SREBP-1c, or Ad-GFP) was added to the medium of primary cultured hepatocytes (1.8×10^7 infection-forming units in 500 μL).

TG/diacylglycerol synthesis in isolated liver and primary hepatocytes. The liver was dissected from tendon to tendon and placed in modified Krebs-Henseleit buffer containing 4% fatty acid-free bovine serum albumin (Sigma-Aldrich), 5 mmol/L glucose, and 0.5 mmol/L palmitate, giving a palmitate-to-bovine serum albumin molar ratio of 1:1. After a 30-min preincubation period, liver strips were transferred to vials containing 0.5 μCi/mL [1-^{14}C]palmitate (GE Healthcare Life Sciences, Buckinghamshire, U.K.) for 60 min. For primary hepatocytes, cells were incubated with [1-^{14}C]palmitate in medium for 6 h. From the liver or cells, lipids were extracted with chloroform/methanol (2:1) and resolved by thin-layer chromatography (hexane/ethyl ether/acetic acid = 60:40:3) followed by photoimaging detection.

Transfection and luciferase assay with methylated plasmids. A luciferase gene construct containing the *Gpam* promoter fragment (from −489 to +79, taking the first nucleotide of exon 1 as +1) was prepared. For in vitro DNA methylation, the construct was digested with *Asp*718/*Xho*I, and a fragment containing the *Gpam* promoter (−489 to +79) was purified, which was followed by treatment with *Sss*I (CpG methylase) as described previously (17). Methylation was confirmed by digestion with a methylation-sensitive restriction enzyme, *Hpa*II. The luciferase assay was performed as described in (19,24).

Chromatin immunoprecipitation analysis. Chromatin immunoprecipitation (ChIP) was performed using an assay kit (Upstate, Temecula, CA) (25). The lysate was incubated with DynaBeads protein G-conjugated (Life Technologies, Carlsbad, CA) anti–SREBP-1c (sc-8984X; Santa Cruz Biotechnology), anti-Dnmt1 (sc-20701; Santa Cruz Biotechnology), anti-Dnmt3a (ab2850; Abcam), anti-Dnmt3b (ab2851; Abcam), anti-trimethyl-histone H3 (Lys4) (#07-473; Upstate), anti-acetyl-histone H3 (Lys9) (#06-911; Millipore, Temecula, CA), anti-dimethyl-histone H3 (Lys9) (#9753; Cell Signaling Technology, Danvers, MA) antibody, or rabbit normal IgG (sc-2027; Santa Cruz Biotechnology). The ChIP-enriched DNA samples were analyzed by quantitative PCR. PCR primers were designed to locate SREs of the *Gpam* or *Scd1* promoter (Supplementary Table 3).

Liver TG analysis. The liver TG levels were measured by enzymatic colorimetry as described (19).

Statistical analysis. Statistical analysis was performed using Student *t* test and ANOVA followed by Scheffe test. Data were expressed as the mean ± SE. A P value of <0.05 was considered statistically significant.

RESULTS

Lipogenic gene and SREBP-1c mRNA expression in the neonatal and adult livers. We examined lipogenic gene expression in the neonatal and adult livers before and after weaning. The GPAT1 mRNA was only slightly expressed in the neonatal liver (days 0, 5, and 9), but markedly increased (~40-fold) in the adult liver (10 weeks of age). Similar to GPAT1, both SCD1 and FAS mRNA levels, as well as protein levels of GPAT1, SCD1, and FAS, and GPAT-mediated TG/diacylglycerol (DG) biosynthesis were increased in the adult liver relative to the neonatal liver (Fig. 1*A* and Supplementary Fig. 2). There is a GPAT1 splicing-variant (GPAT1-variant) with an alternative first noncoding exon (GenBank accession number: NM_008149) using an alternative promoter that is ~30 kb downstream from the *Gpam* promoter containing SREs, thus producing the identical coding GPAT1 protein. In this study, its mRNA expression showed a relatively small increase (approximately threefold) from neonates (day 0) to adults (Fig. 1*A*).

SREBP-1c mRNA was weakly expressed in the neonatal liver (day 0) and increased markedly (~100-fold) in the adult liver (10 weeks of age). At day 9, approximately half the level seen in the adults was observed (Fig. 1*A*). SREBP-1c protein level was very low on day 0 and modestly and markedly increased on day 9 and in adults, respectively (Fig. 1*A*). Namely, on day 9, SREBP-1c was expressed but its target genes were not; they showed delayed expression than SREBP-1c, suggesting that the activity of SREBP-1c is regulated posttranslationally.

DNA methylation of lipogenic gene promoters in neonatal and adult livers. The *Gpam* promoter region contains three SREs (Fig. 1*B*) (6). Bisulfite analysis revealed high DNA methylation levels of the *Gpam* promoter containing SREs in the neonatal liver (day 0) (Fig. 1*C*). By contrast, less DNA methylation levels were observed in the adult liver (Fig. 1*C*). We also confirmed the differential DNA methylation of the *Gpam* promoter in the neonatal and adult livers, based upon digestion with a methylation-sensitive enzyme, *Hpa*II, for which the recognition site locates between the first and second SREs (Fig. 1*B*), and a subsequent quantitative real-time PCR analysis. Consistent with the data of bisulfite analysis, DNA methylation levels were high in the neonatal liver (day 0 and 5; ~60%, day 9; ~55%) relative to the adult liver (~15%) (Fig. 1*D*). By contrast, appreciable DNA methylation of the *Scd1* and *Fasn* promoters, containing SREs, was not observed in both the neonatal (day 0) and adult (10 weeks of age) livers (Fig. 1*E*).

In a CpG island of the alternative promoter of the *Gpam*, there was also no significant DNA methylation in the neonatal (day 0) and adult (10 weeks of age) livers (Fig. 1*E*). In contrast, DNA methylation levels were high in the repetitive element of intracisternal A particle (IAP) (26), one of the markers of global DNA methylation, in both the neonatal and adult livers (Fig. 1*E*). It is therefore likely that DNA methylation differs in certain regions of the genome between neonatal and adult livers.

DNA methylation of the *Gpam* promoters in the adult skeletal muscle. In contrast to the liver, high DNA methylation levels in the *Gpam* promoter were observed in

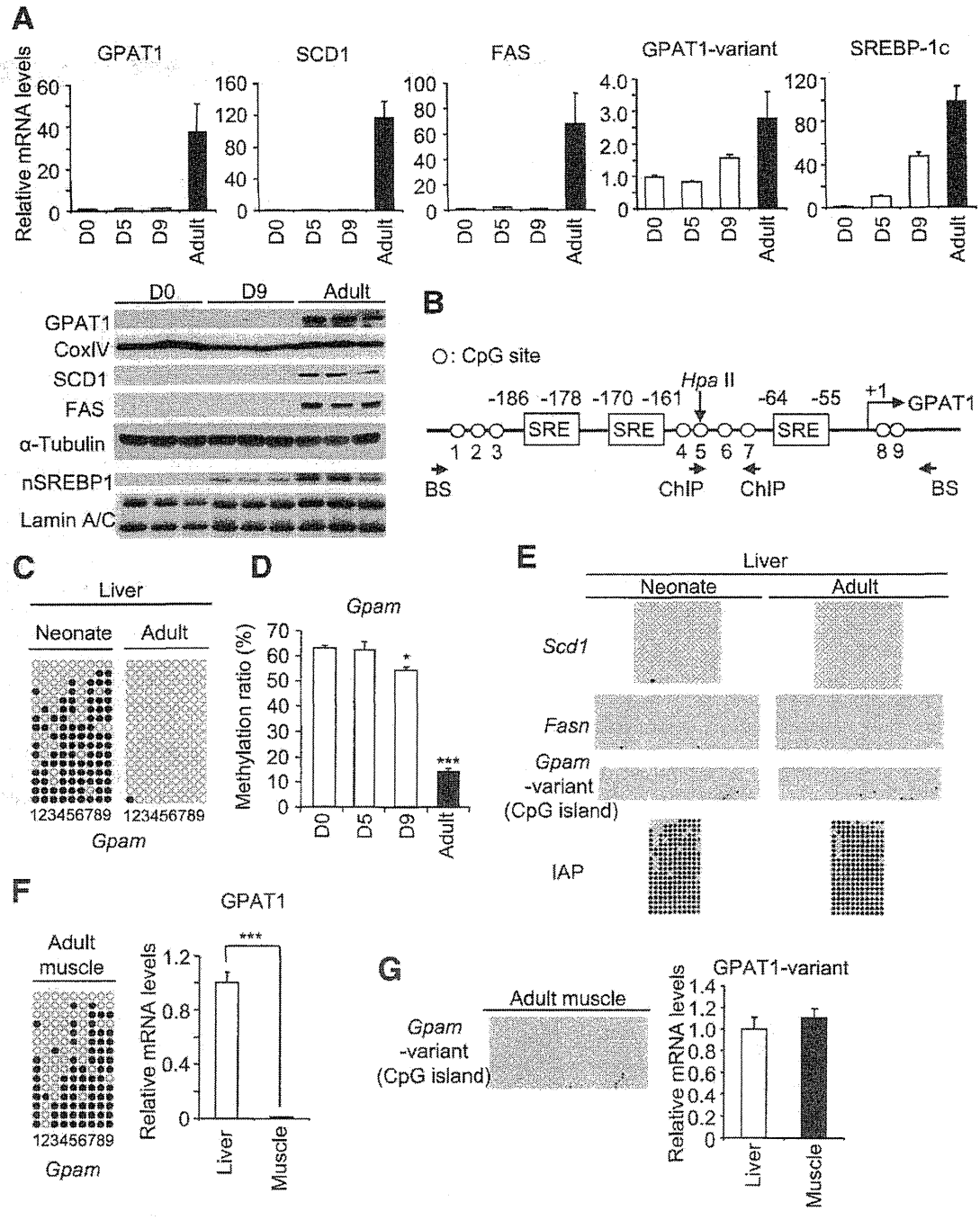

FIG. 1. Lipogenic gene expression and DNA methylation in the neonatal and adult mice livers. *A*: Relative lipogenic gene and SREBP-1c mRNA levels in the neonatal (days after birth: 0, 5, and 9) and adult livers (after weaning, 10 weeks of age), examined by quantitative real-time PCR. Values for day 0 were set at 1. Western blot analysis of GPAT1, SCD1, FAS, and nuclear form of SREBP-1 (nSREBP1) in neonatal (days 0 and 9) and adult livers (10 weeks of age). For GPAT1, mitochondrial fraction was used. For FAS/SCD1 and SREBP-1, cytoplasmic and nuclear fractions were used, respectively. α-Tubulin and Lamin a/c are cytoplasmic and nuclear markers, respectively, used for loading controls. *B*: Schematic representation of the *Gpam* promoter region. The *Gpam* promoter contains three SREs (−186 to −178, −170 to −161, and −64 to −55, transcription start site counted as +1). Each circle denotes a CpG site, numbered 1–9. The *Hpa*II site is indicated (arrow). Position of PCR primers for bisulfite PCR analysis (BS) and ChIP analysis are indicated. *C*: Bisulfite analysis of the *Gpam* promoter. PCR primers used in bisulfite analysis for the *Gpam* promoter are shown in *B*. Filled circles are methylated and open circles are unmethylated CpGs. The numbers beneath are as shown in *B*. The *left panel* is a neonatal liver sample (day 0), and the *right panel* is an adult liver sample (10 weeks of age). Representative results of three independent animals of each group with similar results are shown. *D*: DNA methylation of the *Gpam* promoter, estimated by *Hpa*II digestion followed by quantitative real-time PCR. Genomic DNA treated with *BamH*I alone was prepared as an uncut control (i.e., a fully methylated control [100%]) and diluted as a standard dilution series. $^{*}P < 0.05$, $^{***}P < 0.001$ compared with D0 sample; $n = 3$. *E*: Bisulfite analysis of the *Scd1* and *Fasn* promoters and the alternative *Gpam* promoter, containing CpG island, and IAP in the neonatal and adult liver. Representative results of three independent animals of each group with similar results are shown. *F*: Bisulfite analysis and quantitative real-time PCR mRNA analysis of the *Gpam* promoter in the adult skeletal muscle (10 weeks of age). Values for the liver were set at 1. $n = 3$. For bisulfite analysis, a typical result from three independent experiments with similar results is shown. $^{***}P < 0.001$. *G*: Bisulfite analysis of the alternative *Gpam* promoter in the adult skeletal muscle and relative GPAT1-variant mRNA levels in the adult liver and skeletal muscle. $n = 3$. CoxIV, cytochrome oxidase IV, a mitochondrial marker.